CENTRO DE INVESTIGACIONES
EN OPTICA, A.C.

First-principles calculation of the electronic and optical properties in nanoscopic systems

by

Alejandra Martínez Aceves

A thesis submitted in conformity with the requirements
for the degree of Maestro en Ciencias

Centro Universitario de la Ciénega
Universidad de Guadalajara

July, 2017

Advisor:

Dr. César Castillo Quevedo
Centro Universitario de la Ciénega. Universidad de Guadalajara.

Co-Advisor:

Dr. Norberto Arzate Plata
Centro de Investigaciones en Óptica, A.C.

Thesis committee:

Dr. Jorge Enrique Mejía Sánchez
Centro Universitario de los Lagos. Universidad de Guadalajara.

Dra. María Eugenia Sánchez Morales
Centro Universitario de la Ciénega. Universidad de Guadalajara.

Dr. Cuauhtémoc Acosta Lua
Centro Universitario de la Ciénega. Universidad de Guadalajara.

Dr. Diego Ulises Carranza Sahagún
Centro Universitario de la Ciénega. Universidad de Guadalajara.

For my father and my mother, as
well as for my boyfriend.

Contents

List of Figures

List of Tables

Acknowledgements

This project has been partly supported by CONACYT, No. 663108 and the computing resources used in this work were partly provided by Centro de Investigaciones en Óptica, A. C.

I would especially like to acknowledge Dr. Norberto Arzate Plata for his invaluable assistance in the process for the research done for this project as well as for his help during the course of this thesis. He is an example of life and I have learned a lot from his philosophy. Also I am thankful for all that he has shared with me, of course, I have obtained knowledge from him as I have been learning to handle the computational tools as well as I have been learning from the electronics and the optics.

Secondly I would like to thank Dr. César Castillo Quevedo because thanks to him I met this world of science materials. I obtained a huge amount of experience academically as well as in my personal development. He taught me physics and mathematics from the most basic to the most complex. Not least important to my teachers who are: Dra. Maria Eugenia Sánchez Morales, Dr. Cuauhtémoc Acosta Lua, Dr. Diego Ulises Carranza Sahagún for the knowledge they shared as well as for the personal growth provided. Another great and special thanks to Dr. Alberto Rubio P. for recieving me in the UAM as well as for giving me assistance and giving me access to the computer softwares. To Dr. José Luis Cabellos because he helped me get together the requirements to enroll including the proposal for the research topic.

Last but not least, most importantly, I would like to thank my parents Alberto Martínez Navarro and Luz María Aceves Arias, the two most important people in my life. I have always been taught by them to be a person with good principles. I also thank my brothers who are Alberto, Luz María and Andrés because they have always been there for me and are witness of my growth and part of my achievements. Another acknowledgement

is to my cousin Jessica Ruíz for her support with my second language and assistance in my thesis.
To my boyfriend Osvaldo Ramírez Vázquez, I am thankful for his unconditional support and confidence also for being with me during this process. This concluded stage is an achievement shared by both. He helps me to be a better person. Of course I also thank the tremendous family of momentum-pro for their special support and for promoting my fundamental values of life.
A big thank you for Paulo González Madrid y Aceves, he is a very special person. He supported me during my journey in obtaining my masters degree. He has given me advice and he has been part of my development.
In conclusion, I owe my achivemnets to all this wonderfull people for always being suportive and being there for me.

Abstract

In the present study, we investigate the electronic properties and optical response of armchair graphane nanoribbons (NRs). They have shown to exhibit potential applications such as nanoscale-optical materials, optoelectronics devices and transistors. We have perfomed first principles calculation for the linear optical response with the use of Density Functional Theory (DFT) within the Local Density Approximation (LDA). We have obtained the electronic band structures of graphane systems and of the following armchair graphane NRs: C_6H_{10}, $C_{10}H_{14}$, $C_{14}H_{18}$, $C_{18}H_{22}$. Furthermore, we have obtained the respective spectra for the real and imaginary parts of the dielectric function. We have found that, graphane and the graphane NRs are semiconductor materials, in contrast to graphite and graphene which are conductor materials. The band gap energy of armchair graphane NRs decreases as the width of the NR increases. We also found that the magnitude of the imaginary part of the dielectric function of graphane NRs shows a general decreasing of its magnitude in the whole range of frequencies as the NR width reduces. Besides, our results show that the optical response of graphane NRs is anisotropic.

Chapter 1

Introduction

In the past years, a new class of materials has been discovered called two-dimensional (2D) crystals. Among them, there is graphene, which is a carbon-based system. It is a single planar sheet of sp^2-bonded carbon atoms with a hexagonal Bravais lattice structure. The graphene monolayers were discovered by Geim and Novoselov in 2004 [1](**Novoselov2004**). They obtained experimentally few monolayer samples of graphene including that of one monolayer by the method of mechanical exfolliation [1](**Novoselov2004**). Since then there has been great interest on studies of graphene or graphene-like 2D materiales that contain one or few atomic monolayers. In general, their physical properties depend largely on their dimensions. The graphene structures show electronic properties quiet different from their respective bulk structures[2, 3](**Novoselov2005,Xia2014**),[4, 5](**Xia2014b,Morpurgo2015**). The graphene monolayer is considered to be the basic building block of graphitic materials. Graphite is identified as a three-dimensional (3D) stacking structure from single-carbon-layer structures [6](**Singh2011**). Figure 1.1(a) shows the graphite structure composed of graphene monolayers. It has a Bravais hexagonal lattice. The graphene planar sheet shown in Figure 1.1(b) has two carbon atoms that are within the unit cell. The bond length between carbon atoms from this material is 1.42 Å and its lattice constant is equal to 2.46 Å.

Both graphite and graphene are conductor materials, in other words, it means that they have a zero energy gap between their respective valence and conduction bands. Figure 1.2 shows schematically the band energies of a conductor (a), semiconductor (b), and insulator (c) [7](**Castro2009**). There is a relatively small energy band gap for a semiconductor, while for an insulator the energy band gap is large.

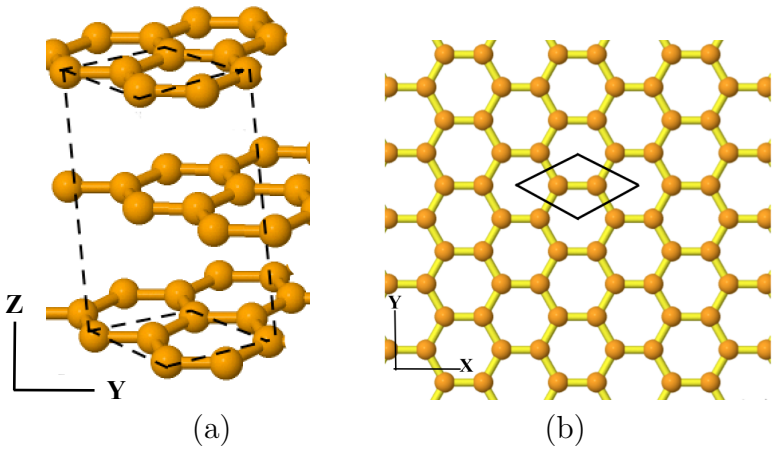

Figure 1.1: Graphite and graphene structures.

After years of research many graphene properties have been measured or calculated. Just a few years ago, researchers reported that graphene have a high charge mobility of μ =230,000 cm^2/Vs, a 3000 W/mK of thermal conductivity, a strength of 130 GPa, a surface area equal to 2600 m^2/g [8](**Mendez2012**). The properties of a single layer, bilayer or few-layers graphene are different but each property from these are used in specific cases [6](**Singh2011**). For example, it was discovered that a thick sample of graphene absorbs 2.3% of the white light from an incident beam, which is and exceptional electronic feature[9](**Nair2008**). The graphene-based materials have amazing electronic and structural properties including high electrical and thermal conductivities as well as unique optical properties and chemical stability. Graphene has been impacted by the importance of technology applications including transparent and flexible electronics, capacitors, batteries, transistors, data storage, sensors, printable inks, barrior materials, microelectromechanical systems, nanoelectromechanical systems and nanocomposites [10](**Castro2011**) [11](**Rodriguez2015**).

Few-layer graphene structures also show interesting properties. For example, the bilayer graphene exhibits a gate-tunable band gap. [12](**Castro2007**) Meanwhile the trilayer graphene is a semimetal with a gate tunable overlap between the conduction and the bands. Recently, it has been theoretically suggested the electronic properties depend on the number of layers and on layer stacking. For instance, high transparency or perfect reflection depends on the graphene system structure.

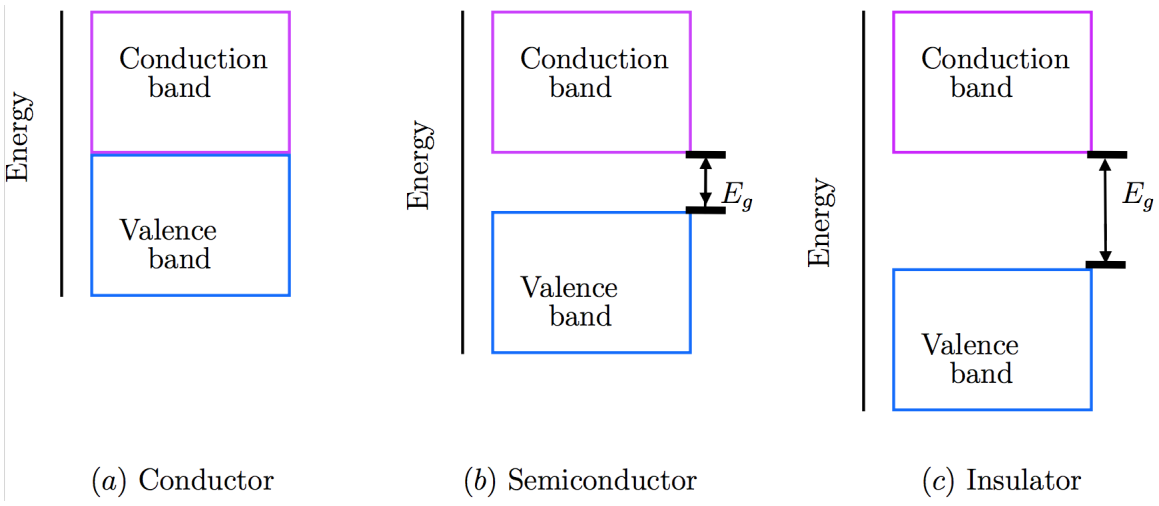

Figure 1.2: Scheme of the energy bands of: (a) conductor, (b) semiconductor and (c) insulator.

Efforts have been made to open tha band gap in graphene. This will make graphene interesting because of the potential optoelectronic applications it will have. For instance, when a perpendicular electric field is applied on graphene, the result is to open the band gap but this affects the pseudospin from the charge carriers. A conceptually novel construction is the use of the pseudospin, proposed by theoretical schemes that find the posibility to get pseudospintronic devices[13](**Sahhin2015**). Another method that have been used in order to modify the electronic properties of graphene is by the adsorption of foreign atoms on the graphene sheet. For example, boron, nitrogen or hydrogen atoms can be adsorbed on graphene. The respective band structure has been reported in experimental studies by substitution of atoms or by adsorption of foreign atoms in the surface of graphene [14](**Craciun2009**).

Graphane is the structure composed of a planar sheet of sp^3-bonded carbon atoms where every carbon atom bonds to one hydrogen atom. This system was called that way by Sofo et al., in 2007 [15](**Sofo2007**). The chair, boat, stirrup, armchair and twist-boat structures are various of their possible configurations. The chair structure is the most stable [15](**Sofo2007**). Unlike graphene, graphane is a semiconductor material. It means that there is an energy band gap between the highest valence band and the lowest conduction band. The energy band gaps are 3.5 and 3.7 eV for the chair and boat structures, respectively.

The experimental synthesis of graphane was performed by Elias et al., in 2009 [16](**Elias2009**). They used three samples of graphene crystals for their hydrogenation.

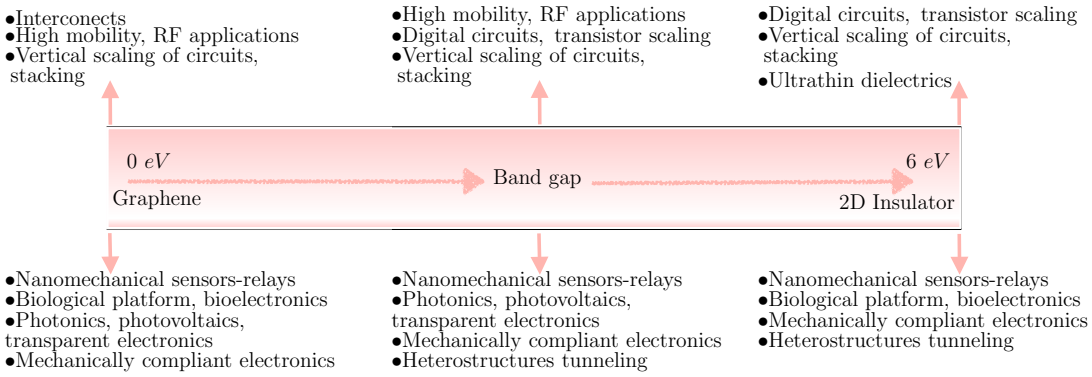

Figure 1.3: Technological applications of carbon-based structures depending on their band gap energy [13](**Sahhin2015**).

These samples were exposed to a cold hydrogen plasma with low-pressure (0.1 mbar) hydrogen-argon mixture of 10% H_2 and with dc plasma ignited between two aluminum electrodes. In order to avoid a possible damage by energetic ions they kept the samples 30 cm away from the discharge zone. The plasma treatment to reach the saturation required 2 hours and they corroborated the changes induced by hydrogenation through Raman spectroscopy [16](**Elias2009**).

Their technological applications are possible through the control of its electronic and optical properties. Graphane has potential technological applications. For example, the H_2-storage in nano scale, design of thermoelectric applications through the stability of their atomic binding, as well as their low cost and easy synthesis. The characteristics of geometric structures as the bond lengths, angles, and rise of carbon atoms, markedly depend on the concentration and distribution of hydrogen atoms. [17](**Huang2016**). Figure 1.3 shows different technological applications that carbon-based structures might have depending on their band gap energy [18](**Sahin2015**).

Graphane can be cut into large narrow atomic stripes or bands called nanoribbons (NRs). The graphane NRs are classified according to the orientation of the atomic bands or termination of the atomic edges as armchair and zigzag structures[19](**Ataca2010**). An example of graphane NRs structure is shown in Figure 1.4. In this 2D graphane structures, the electronic and optical properties are modified as a result of the shortening of their dimensions. For instance, their band gap energy increases[18](**Sahin2015**). Besides, their band gap energy depends on the hydrogenation percentage. The electronic and magnetic properties of graphane NRs have been studied but there are few studies of their optical properties [20](**Yang2012**). The increase of graphane energy band gap exhibits possible applications in nano scale materials, optoelectronics and transistors.

The study of the optical and electronic properties of graphane NRs is fundamental for their characterization and possible applications [21](**Hu2015**).

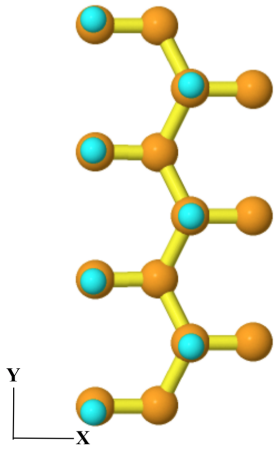

Figure 1.4: Unit cell of a graphane NR. Hydrogen and carbon atoms are indicated by blue and orange spheres, respectively

1.1 Objectives

The objectives of this thesis are based on the study of the electronic structure and linear optical response of nanoscopic systems based on graphene. Calculations of energy band structure, and dielectric function of the studied structures are performed. The calculations are based on Density Functional Theory (DFT).

1.1.1 General objective

The general objective of this thesis is:

- To characterize the electronic and optical properties of nanoscopic systems based on graphene by first principle calculations.

1.1.2 Specific objectives

To achieve the general objective we propose the following specific objectives:

- To calculate the electronic structure and optical response of graphane nanostructures based on DFT calculations and using pseudopotentials.
- To obtain the ground state structure of the following graphane NRs: C_6H_{10}, $C_{10}H_{14}$, $C_{14}H_{18}$, $C_{18}H_{22}$.
- To determine the electronic band structure and linear optical response of C_6H_{10}, $C_{10}H_{14}$, $C_{14}H_{18}$, $C_{18}H_{22}$ graphane NRs.

1.2 Hypothesis

Graphene is an isotropic material, meanwhile a graphene-based NRs are anisotropic. Thus an anisotropic optical response is expected in graphane NRs. Therefore, we propose the following hypothesis of investigation:

- The optical response of graphane nanostructures in the form of NRs is anisotropic, and their band gap energy depends on their lateral size.

1.3 Justification

The optical responses of graphane NRs are very important for designing electronics devices with a high technological potential. Additional properties of they can be obtained through edges hydrogenization, adatom adsorption, vacancy creation, edge profiling, and superlattices[19](**Ataca2010**). Nevertheless, graphane NRs on their optical properties there are few research and it have remained unexplored. Due to their optical properties they are suitable for diverse applications such as nanoscale-optical and optoelectronic devices[20](**Yang2012**).

1.4 Outline of the thesis

We present in Chapter 2 the crystal structure and the hexagonal lattice as well the vectors of the graphite, graphene, graphane and graphane NRs. Also we have shown their atomic positions and the atomic structure for each system. In Chapter 3 we developed the methodology of first principles and the operation of the computational tool. The band structure of each system and their band gap energy is shown in Chapter 4. We have shown the optical response of the graphane and graphane NRs such as the imaginary portion, ε_2, of the dielectric function in Chapter 5 and finally we conclude in Chapter 6.

Chapter 2

Atomic crystals

2.1 Crystal lattice

An atomic crystal lattice is a periodic ordered arrangement of a group of atoms in space. This group is known as basis and form a unit cell. Thus the translation in space of this cell maps the whole crystal lattice called Bravais lattice. A primitive cell is that of with the minimum volume cell. A Wigner-Seitz cell is a primitive cell centered on a lattice point, in other words it the most compact cell that is symmetric around the origin. The procedure to find it is: firstable, take any lattice point, secondable, draw a line to all nearby lattice points. Then a normal plane is drawn to these lines. The Wigner-Seitz cell is that enclosed region formed by the volume bounded by these planes. In reciprocal space the corresponding cell is known as a Brillouin zone (BZ).

The crystal lattice is formed by a set of infinite lattice points that replace and represent each group of atoms. Every lattice point $\mathbf{R}$ can be found in space by three translational vectors $\mathbf{a}_1, \mathbf{a}_2$ and $\mathbf{a}_3$ in the form

$$\mathbf{R} = l\mathbf{a}_1 + n\mathbf{a}_2 + m\mathbf{a}_3, \tag{2.1}$$

where l, n, m are integers. Hence, the unit cell is characterized by the magnitude of the translational vectors and the angles between the translational vectors. Depending of their values seven different crystal systems are formed: cubic, hexagonal, trigonal, tetragonal, ortorrombic, monoclinic and triclinic. In a two-dimensional (2D) space, there are four

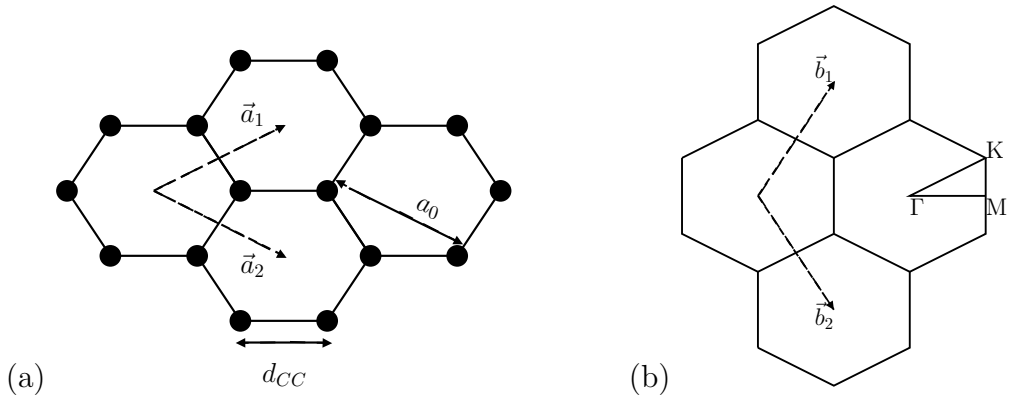

Figure 2.1: Real (a) and reciprocal (b) lattices for the 2D hexagonal structure of graphene. In (a), the translational lattice vectors are shown by $\mathbf{a}_1$, and $\mathbf{a}_2$; a_0 is the lattice constant, and d_{CC} is the carbon-carbon distance. In (b), translational reciprocal lattice vectors are shown by $\mathbf{b}_1$, and $\mathbf{b}_2$. Γ, M and K are special wave vector points, which define the irreducible Brillouin zone.

crystal systems: squared, rectangular, centered rectangular, hexagonal and oblique. For instance, in Figure 2.1(a), we can see the 2D hexagonal lattice for graphene.

2.2 Reciprocal lattice

The reciprocal lattice is that lattice formed in momentum space or $\mathbf{k}$ space. The real and reciprocal lattices are Fourier transform of each other. In crystallography, the reciprocal lattice of a Bravais lattice is a set of all $\mathbf{K}$ points such that the following expression

$$e^{i\mathbf{K}\cdot\mathbf{R}} = 1 \tag{2.2}$$

is satisfied for all real lattice points $\mathbf{R}$. The corresponding reciprocal translation vectors are obtained by the expressions

$$\mathbf{b}_1 = 2\pi\frac{\mathbf{a}_2\times\mathbf{a}_3}{\mathbf{a}_1\cdot|(\mathbf{a}_2\times\mathbf{a}_3)|}; \qquad \mathbf{b}_2 = 2\pi\frac{\mathbf{a}_3\times\mathbf{a}_1}{\mathbf{a}_1\cdot|(\mathbf{a}_2\times\mathbf{a}_3)|}; \qquad \mathbf{b}_3 = 2\pi\frac{\mathbf{a}_1\times\mathbf{a}_2}{\mathbf{a}_1\cdot|(\mathbf{a}_2\times\mathbf{a}_3)|}. \tag{2.3}$$

Hence, every reciprocal lattice point $\mathbf{K}$ can be found in space by the use of the reciprocal translational vectors $\mathbf{b}_1, \mathbf{b}_2$ and $\mathbf{b}_3$ in the form

$$\mathbf{K} = p\mathbf{b}_1 + q\mathbf{b}_2 + s\mathbf{b}_3, \tag{2.4}$$

where p, q, s are integers. In Figure 2.1(b), the reciprocal lattice is shown. The translational reciprocal lattice vectors are indicated as well as the special $\mathbf{k}$ points, Γ, M and K, that define the irreducible BZ.

2.3 Graphite

Graphite is a three-dimensional (3D) atomic layered structure formed by carbon atoms. Its crystal symmetry is hexagonal and belongs to the space group $P6_3/mmc$. The carbon atoms on the plane of the layer bond covalently by sp^2 hybridization of atomic orbitals called σ orbitals. Meanwhile, the carbon layers are weakly bonded by Wan der Vals forces that arise from nonhybridized p_z orbitals called π orbitals that are perpendicular to the graphitic planes. The graphite structure is shown in Figure 2.2. Two consecutive layer are shifted to each other, such that its stacking is of the form AB AB. The unit cell of graphite is shown in Figure 2.2(b). There are four carbon atoms per unit cell. The interatomic bonding is d_{C-C} =1.42 Å and its in-plane lattice constant a_0 is equal to 2.46 Å due to: $a_0 = |\mathbf{a}_1| = |\mathbf{a}_2| = \sqrt{3}\, d_{C-C} = 2.46$ Å. The length between sheets is of 3.35 Å and the out-of-plane lattice constant is $c_0 = 6.7$ Å.

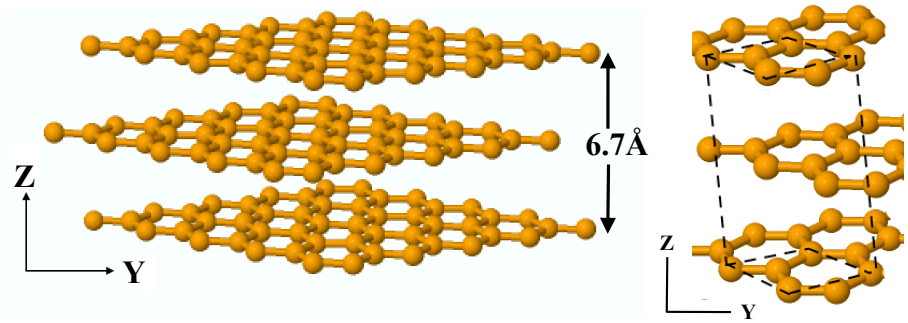

Figure 2.2: Atomic structure of graphite (a) and its unit cell (b).

The primitive translational lattice vectors in real space $\mathbf{a}_1$, $\mathbf{a}_2$ and $\mathbf{a}_3$ of graphite are:

$$\mathbf{a_1} = a_0(\sqrt{3}, \frac{1}{2}, 0), \tag{2.5}$$

$$\mathbf{a_2} = a_0(\sqrt{3}, -\frac{1}{2}, 0), \tag{2.6}$$

$$\mathbf{a_3} = c_0(0, 0, 1). \tag{2.7}$$

The corresponding primitive lattice vectors in reciprocal space $\mathbf{b}_1$, $\mathbf{b}_2$ and $\mathbf{b}_3$ of graphite are:

$$\mathbf{b_1} = \frac{2\pi}{a_0}(\frac{1}{\sqrt{3}}, 1, 0), \tag{2.8}$$

$$\mathbf{b_2} = \frac{2\pi}{a_0}(\frac{1}{\sqrt{3}}, -1, 0), \tag{2.9}$$

$$\mathbf{b_3} = \frac{2\pi}{c_0}(0, 0, 1). \tag{2.10}$$

2.4 Graphene

Graphene is identified as a two-dimensional (2D) structure formed by one atomic plane of the graphite structure. The graphene structure is shown in Figure 2.3. This material has two carbon atoms per unit cell, which is indicated by the rectangle in black in Figure 2.3. We calculated an interatomic bonding of 1.42 Å and their lattice constant is equal to 2.443 Å. Our results were compared with reported values. We got a good comparison. The results obtained by Sahin et al., [7](**Castro2009**) are 1.42 Å for the bond length between carbon atoms and 2.46 Å for the lattice constant.

The primitive translational lattice vectors $\mathbf{a}_1$ and $\mathbf{a}_2$ of graphene are

$$\mathbf{a_1} = a_0(\sqrt{3}, \frac{1}{2}), \tag{2.11}$$

$$\mathbf{a_2} = a_0(\sqrt{3}, -\frac{1}{2}). \tag{2.12}$$

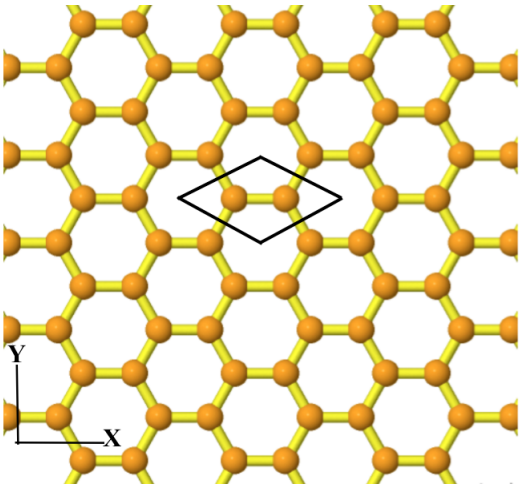

Figure 2.3: Graphene structure. The unit cell is indicated by the rectangle in black

The primitive reciprocal translational lattice vectors $\mathbf{b}_1$ and $\mathbf{b}_2$ for graphene are

$$\mathbf{b_1} = \frac{2\pi}{a_0}(\frac{1}{\sqrt{3}}, 1), \tag{2.13}$$

$$\mathbf{b_2} = \frac{2\pi}{a_0}(\frac{1}{\sqrt{3}}, -1). \tag{2.14}$$

2.5 Graphane

Graphane is identified as a two-dimensional (2D) structure formed by the adsorption of hydrogen atoms on the graphene structure. There is one hydrogen atom bonding to each carbon atom. There are seven reported isomers of graphane or possible graphane atomic configurations: chair, boat, stirrup, armchair, TB-chair, twist-boat, and tricycle [18]. The most stable configuration is the chair graphane structure. In this configuration, the hydrogen atoms bond alternately above and below to carbon atoms. Figure 2.4 shows the perspective and top views of graphane. In the following, we consider the chair configuration for graphane. This material has two carbon atoms and two hydrogen atoms per unit cell. Figure 2.5 shows the atomic unit that forms the unit cell. The sp^2 bonding on graphene is converted to sp^3 bonding on graphane through the hydrogen-carbon bonds.

The space group of the chair configuration is P-$3m1$, number 164. The bond length between carbon atoms (d_{CC}) of this material is (d_{CC}) = 1.536 Å, the carbon-hydrogen bond length is (d_{CH}) = 1.104 Å, and the respective lattice constant is a_0 = 2.539 Å

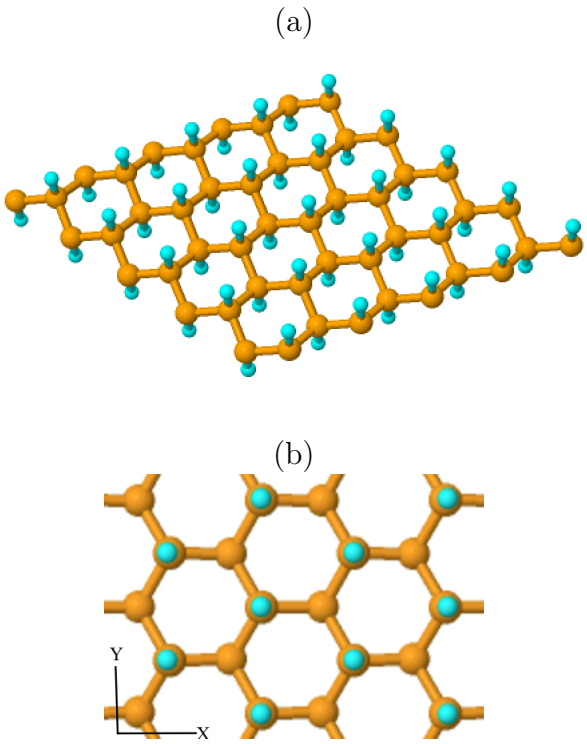

Figure 2.4: Perspective (a) and top (b) views of the graphane structure. Carbon (hydrogen) atoms are indicated by balls in orange (blue).

[13](**Sahhin2015**). Although, the results reported by Sofo et al., [15] are the following: d_{CC} =1.52 Å, d_{CH} =1.11 Å and the lattice constant $a_0 = 2.516$ Å.

The primitive translation lattice vectors $\mathbf{a}_1$ and $\mathbf{a}_2$ for graphane are

$$\mathbf{a_1} = a_0(\sqrt{3}, \frac{1}{2}), \tag{2.15}$$

$$\mathbf{a_2} = a_0(\sqrt{3}, -\frac{1}{2}). \tag{2.16}$$

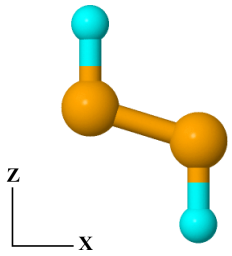

Figure 2.5: The atomic unit that forms the unit cell of graphane. Carbon (hydrogen) atoms are indicated by balls in orange (blue).

	x	y	z
C_1	1.44626	0.00000	0.22335
C_2	2.89252	0.00000	-0.22335
H_1	1.44626	0.00000	1.33981
H_2	2.89252	0.00000	-1.33981

Table 2.1: Atomic positions for graphane in Å.

The primitive reciprocal lattice vectors $\mathbf{b}_1$ and $\mathbf{b}_2$ for graphane are

$$\mathbf{b_1} = \frac{2\pi}{a_0}(\frac{1}{\sqrt{3}}, 1), \tag{2.17}$$

$$\mathbf{b_2} = \frac{2\pi}{a_0}(\frac{1}{\sqrt{3}}, -1). \tag{2.18}$$

We have calculated the corresponding geometric atomic structure of graphane through first principles calculation. For that, we have minimized the total energy and done a convergence study. We have obtain the atomic positions in Å of graphane, which are shown in Table 2.1. We also obtained the following results fo the bond lenghts and lattice constant: $d_{CC} = 1.5137$ Å, $d_{CH} = 1.1164$ Å, $a_0 = 2.505$ Å.

2.6 Graphane nanoribbons

Two-dimensional (2D) graphane structures recieve the name of nanoribbons (NRs) when one of the lateral sizes of graphane is finite, that is it has a finite width. Meanwhile, the other perpedicular lateral size keeps being infinite. Hence, NRs can be consider as a one-dimensional (1D) structures. Graphane NRs can be classified depending on their orientation in armchair and zigzag configurations [19](**Ataca2010**). The width M of the armchair graphane NRs is defined by the number of C-C dimers in the unit cell which is parallel to the axis of the nanoribbon (NR). Figure 2.6 shows the side view of a chair graphane NR of width M. The axis of the NR is along the x direction.

The primitive translation vector of a graphane NR $\mathbf{a}_1$ is

$$\mathbf{a}_1 = (1, 0, 0)a_0. \tag{2.19}$$

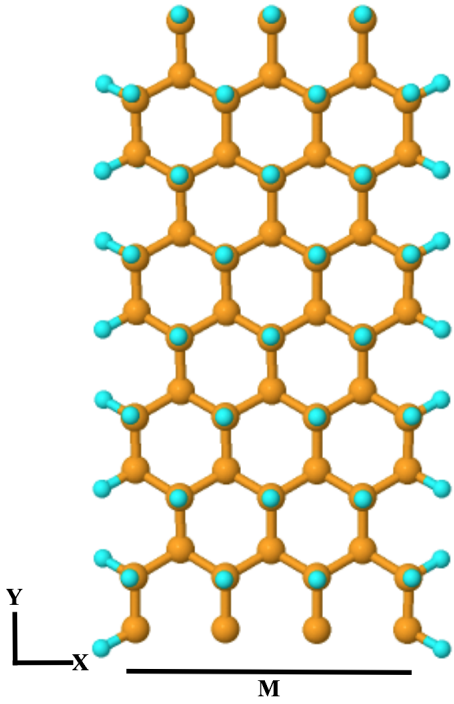

Figure 2.6: Top view of the atomic structure of a chair graphane NR of width M. Carbon (hydrogen) atoms are indicated by balls in orange (blue).

where a_0 is the lattice constant.

The primitive reciprocal lattice vector $\mathbf{b}_1$ of a graphane NRs is

$$\mathbf{b}_1 = \frac{2\pi}{a_0}(1, 0, 0). \tag{2.20}$$

The graphane NRs can be bare or passivated with hydrogen at the edges. This has the effect of removing the charge density at the edges of the NR due to edge state bands [19](**Ataca2010**). In our study , we consider graphane NR passivated with hydrogen at the edges. The studied atomic NRs structures are: C_6H_{10}, $C_{10}H_{14}$, $C_{14}H_{18}$, and $C_{18}H_{22}$. Their respective atomic unit cell arrangements are shown in Figure 2.7.

We have perfomed first principles calculations for minimizing the total energy of these structures, and obtained their lattice constant and corresponding atomic positions. A convergence study was done. The C_6H_{10} graphane NR has sixteen atoms in its unit

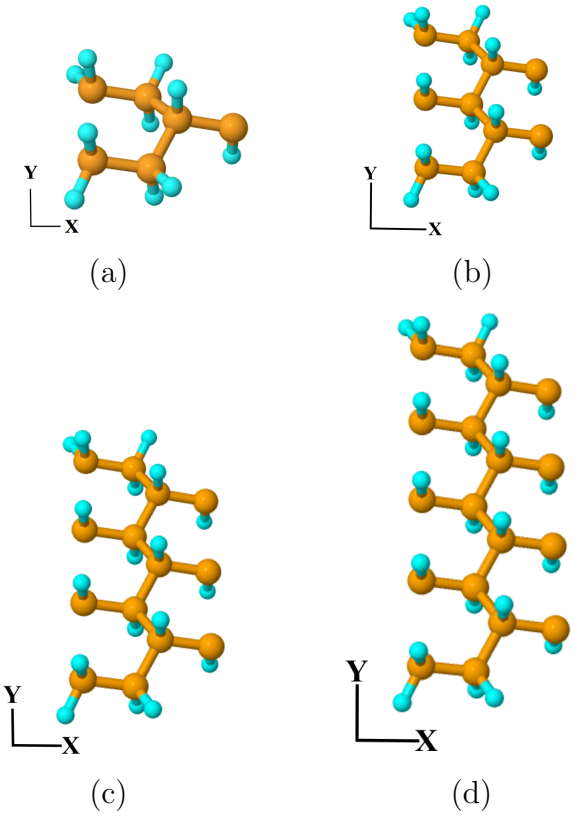

Figure 2.7: Atomic unit cell of armchair graphane NRs: (a) C_6H_{10}, (b) $C_{10}H_{14}$, (c) $C_{14}H_{18}$, and (d) $C_{18}H_{22}$. Carbon and hydrogen atoms are shown by balls in orange and blue, respectively.

cell. The calculated lattice constant is a_1 =4.4115 Å and the width of this structure is a_2 =12.5224 Å . The atomic positions and bond lengths in Å of this structure are shown in Table 2.2. The $C_{10}H_{14}$ graphane NR has twenty-four atoms in its unit cell. The lattice constant we calculated is a_1 =4.3752 Å and the width of this structure is a_2 =15.0185 Å . The atomic positions and bond lengths in Å of this structure are shown in Table 2.3. The $C_{14}H_{18}$ graphane NR has thirty-two atoms in its unit cell. The lattice constant we calculated is a_1 =4.3632 Å and the width of this structure is a_2 =17.5279 Å . The atomic positions and bond lengths in Å of this structure are shown in Table 2.4. The $C_{18}H_{22}$ graphane NR has forty atoms in its unit cell. The lattice constant we calculated is a_1 =4.3573 Å and the width of this structure is a_2 =20.0344 Å . The atomic positions and bond lengths in Å of this structure are shown in Table 2.5.

	x	y	z
C_1	-0.72507	-1.23293	0.21894
C_2	0.72507	-1.23293	-0.21894
C_3	1.48066	0.00000	0.23450
C_4	2.93015	0.00000	-0.23450
C_5	-0.72507	1.23293	0.21894
C_6	0.72507	1.23293	-0.21894
H_1	-0.77468	-1.28320	1.32721
H_2	0.77468	-1.28320	-1.32721
H_3	1.49261	0.00000	1.34869
H_4	2.91821	0.00000	-1.34869
H_5	-0.77468	1.28320	1.32721
H_6	0.77468	1.28320	-1.32721
H_7	-1.22020	2.14657	-0.15075
H_8	1.22020	2.14657	0.15075
H_9	-1.22020	-2.14657	-0.15075
H_{10}	1.22020	-2.14657	0.15075

$d_{C_1-H_{15}} = 1.10298$	$d_{H_7-C_1} = 1.11051$
$d_{C_2-H_{16}} = 1.10298$	$d_{H_8-C_2} = 1.11051$
$d_{C_3-H_9} = 1.11425$	$d_{H_9-C_3} = 1.11425$
$d_{C_4-H_{10}} = 1.11425$	$d_{H_{10}-C_4} = 1.11425$
$d_{C_5-H_{13}} = 1.10298$	$d_{H_{11}-C_5} = 1.11051$
$d_{C_6-H_{14}} = 1.10298$	$d_{H_{12}-C_6} = 1.11051$
$d_{H_{13}-C_5} = 1.10298$	$d_{H_{14}-C_6} = 1.10298$
$d_{H_{15}-C_1} = 1.10298$	$d_{H_{16}-C_2} = 1.10298$

Table 2.2: Atomic positions and bond lengths for the C_6H_{10} graphane NR in Å units

	x	y	z
C_1	-0.71968	-1.23600	0.22168
C_2	0.71968	-1.23600	-0.22168
C_3	1.46303	-0.00014	0.22952
C_4	2.91226	-0.00014	-0.22952
C_5	-0.73048	1.25155	0.22059
C_6	0.73048	1.25155	-0.22059
C_7	1.46303	2.50323	0.22952
C_8	2.91226	2.50323	-0.2295
C_9	-0.71968	3.73910	0.22168
C_{10}	0.71968	3.73910	-0.22168
H_1	-0.76635	-1.28538	1.32939
H_2	0.76635	-1.28538	-1.32939
H_3	1.47031	0.00756	1.34463
H_4	2.90497	0.00756	-1.34463
H_5	-0.73410	1.25155	1.33710
H_6	0.73410	1.25155	-1.33710
H_7	1.47031	2.49554	1.34463
H_8	2.90497	2.49554	-1.34463
H_9	-0.76635	3.78848	1.32939
H_{10}	0.76635	3.78848	-1.32939
H_{11}	-1.21961	4.64895	-0.14845
H_{12}	1.21961	4.64895	0.14845
H_{13}	-1.21961	-2.14586	-0.14845
H_{14}	1.21961	-2.14586	0.14845

$d_{C_1-H_{23}} = 1.10217$	$d_{H_{11}-C_1} = 1.10979$
$d_{C_2-H_{24}} = 1.10217$	$d_{H_{12}-C_2} = 1.10979$
$d_{C_3-H_{13}} = 1.11516$	$d_{H_{13}-C_3} = 1.11516$
$d_{C_4-H_{14}} = 1.11516$	$d_{H_{14}-C_4} = 1.11516$
$d_{C_5-H_{15}} = 1.11652$	$d_{H_{15}-C_5} = 1.11652$
$d_{C_6-H_{16}} = 1.11652$	$d_{H_{16}-C_6} = 1.11652$
$d_{C_7-H_{17}} = 1.11516$	$d_{H_{17}-C_7} = 1.11516$
$d_{C_8-H_{18}} = 1.11516$	$d_{H_{18}-C_8} = 1.11516$
$d_{C_9-H_{21}} = 1.10217$	$d_{H_{19}-C_9} = 1.10979$
$d_{C_{10}-H_{22}} = 1.10217$	$d_{H_{20}-C_{10}} = 1.10979$

Table 2.3: Atomic positions and bond lengths for the $C_{10}H_{14}$ graphane NR in Å units.

	x	y	z
C_1	-0.71899	-1.23744	0.22096
C_2	0.71899	-1.23744	-0.22096
C_3	1.45863	0.00024	0.22931
C_4	2.90466	0.00024	-0.22931
C_5	-0.72753	1.25119	0.22308
C_6	0.72753	1.25119	-0.22308
C_7	1.45463	2.50400	0.22448
C_8	2.90866	2.50400	-0.22448
C_9	-0.72753	3.75681	0.22308
C_{10}	0.72753	3.75681	-0.22308
C_{11}	1.45863	5.00776	0.22931
C_{12}	2.90466	5.00776	-0.22931
C_{13}	-0.71899	6.24543	0.22096
C_{14}	0.71899	6.24543	-0.22096
H_1	-0.76698	-1.28825	1.32853
H_2	0.76698	-1.28825	-1.32853
H_3	1.46513	0.00932	1.34435
H_4	2.89816	0.00932	-1.34435
H_5	-0.72864	1.24714	1.33934
H_6	0.72864	1.24714	-1.33934
H_7	1.45530	2.50400	1.34055
H_8	2.90799	2.50400	-1.34055
H_9	-0.72864	3.76086	1.33934
H_{10}	0.72864	3.76086	-1.33934
H_{11}	1.46513	4.99868	1.34435
H_{12}	2.89816	4.99868	-1.34435
H_{13}	-0.76698	6.29624	1.32853
H_{14}	0.76698	6.29624	-1.32853
H_{15}	-1.21993	7.15353	-0.15170
H_{16}	1.21993	7.15353	0.15170
H_{17}	-1.21993	-2.14553	-0.15170
H_{18}	1.21993	-2.14553	0.15170

$d_{C_1-H_{31}} = 1.10203$	$d_{H_{15}-C_1} = 1.10977$
$d_{C_2-H_{32}} = 1.10203$	$d_{H_{16}-C_2} = 1.10977$
$d_{C_3-H_{17}} = 1.11510$	$d_{H_{17}-C_3} = 1.11510$
$d_{C_4-H_{18}} = 1.11510$	$d_{H_{18}-C_4} = 1.11510$
$d_{C_5-H_{19}} = 1.11626$	$d_{H_{19}-C_5} = 1.11626$
$d_{C_6-H_{20}} = 1.11626$	$d_{H_{20}-C_6} = 1.11626$
$d_{C_7-H_{21}} = 1.11607$	$d_{H_{21}-C_7} = 1.11607$
$d_{C_8-H_{22}} = 1.11607$	$d_{H_{22}-C_8} = 1.11607$
$d_{C_9-H_{23}} = 1.11626$	$d_{H_{23}-C_9} = 1.11626$
$d_{C_{10}-H_{24}} = 1.11626$	$d_{H_{24}-C_{10}} = 1.11626$
$d_{C_{11}-H_{25}} = 1.11510$	$d_{H_{25}-C_{11}} = 1.11510$
$d_{C_{12}-H_{26}} = 1.11510$	$d_{H_{26}-C_{12}} = 1.11510$
$d_{C_{13}-H_{29}} = 1.10203$	$d_{H_{27}-C_{13}} = 1.10977$
$d_{C_{14}-H_{30}} = 1.10203$	$d_{H_{28}-C_{14}} = 1.10977$
$d_{H_{29}-C_{13}} = 1.10203$	$d_{H_{30}-C_{14}} = 1.10203$
$d_{H_{31}-C_1} = 1.10203$	$d_{H_{32}-C_2} = 1.10203$

Table 2.4: Atomic positions and bond lengths for the $C_{14}H_{18}$ graphane NR in Å units.

	x	y	z
C_1	-0.71855	-1.23772	0.22103
C_2	0.71855	-1.23772	-0.22103
C_3	1.45643	0.00057	0.22934
C_4	2.90092	0.00057	-0.22934
C_5	-0.72667	1.25162	0.22313
C_6	0.72667	1.25162	-0.22313
C_7	1.45268	2.50459	0.22452
C_8	2.90467	2.50459	-0.22452
C_9	-0.72567	3.75646	0.22498
C_{10}	0.72567	3.75646	-0.22498
C_{11}	1.45268	5.00833	0.22452
C_{12}	2.90467	5.00833	-0.22452
C_{13}	-0.72667	6.26130	0.22313
C_{14}	0.72667	6.26130	-0.22313
C_{15}	1.45643	7.51235	0.22934
C_{16}	2.90092	7.51235	-0.22934
C_{17}	-0.71855	8.75065	0.22103
C_{18}	0.71855	8.75065	-0.22103
H_1	-0.76694	-1.28936	1.32863
H_2	0.76694	-1.28936	-1.32863
H_3	1.46270	0.00913	1.34444
H_4	2.89466	0.00913	-1.34444
H_5	-0.72800	1.24739	1.33942
H_6	0.72800	1.24739	-1.33942
H_7	1.45297	2.50518	1.34062
H_8	2.90439	2.50518	-1.34062
H_9	-0.72492	3.75646	1.34105
H_{10}	0.72492	3.75646	-1.34105
H_{11}	1.45297	5.00774	1.34062
H_{12}	2.90439	5.00774	-1.34062
H_{13}	-0.72800	6.26553	1.33942
H_{14}	0.72800	6.26553	-1.33942
H_{15}	1.46270	7.50379	1.34444
H_{16}	2.89466	7.50379	-1.34444
H_{17}	-0.76694	8.80228	1.32863
H_{18}	0.76694	8.80228	-1.32863
H_{19}	-1.22015	9.65798	-0.15230
H_{20}	1.22015	9.65798	0.15230
H_{21}	-1.22015	-2.14506	-0.15230
H_{22}	1.22015	-2.14506	0.15230

$d_{C_1-H_{39}} = 1.10192$	$d_{H_{19}-C_1} = 1.10985$
$d_{C_2-H_{40}} = 1.10192$	$d_{H_{20}-C_2} = 1.10985$
$d_{C_3-H_{21}} = 1.11515$	$d_{H_{21}-C_3} = 1.11515$
$d_{C_4-H_{22}} = 1.11515$	$d_{H_{22}-C_4} = 1.11515$
$d_{C_5-H_{23}} = 1.11630$	$d_{H_{23}-C_5} = 1.11630$
$d_{C_6-H_{24}} = 1.11630$	$d_{H_{24}-C_6} = 1.11630$
$d_{C_7-H_{25}} = 1.11611$	$d_{H_{25}-C_7} = 1.11611$
$d_{C_8-H_{26}} = 1.11611$	$d_{H_{26}-C_8} = 1.11611$
$d_{C_9-H_{27}} = 1.11607$	$d_{H_{27}-C_9} = 1.11607$
$d_{C_{10}-H_{28}} = 1.11607$	$d_{H_{28}-C_{10}} = 1.11607$
$d_{C_{11}-H_{29}} = 1.11611$	$d_{H_{29}-C_{11}} = 1.11611$
$d_{C_{12}-H_{30}} = 1.11611$	$d_{H_{30}-C_{12}} = 1.11611$
$d_{C_{13}-H_{31}} = 1.11630$	$d_{H_{31}-C_{13}} = 1.11630$
$d_{C_{14}-H_{32}} = 1.11630$	$d_{H_{32}-C_{14}} = 1.11630$
$d_{C_{15}-H_{33}} = 1.11515$	$d_{H_{33}-C_{15}} = 1.11515$
$d_{C_{16}-H_{34}} = 1.11515$	$d_{H_{34}-C_{16}} = 1.11515$
$d_{C_{17}-H_{37}} = 1.10192$	$d_{H_{35}-C_{17}} = 1.10985$
$d_{C_{18}-H_{38}} = 1.10192$	$d_{H_{36}-C_{18}} = 1.10985$
$d_{H_{37}-C_{17}} = 1.10192$	$d_{H_{38}-C_{18}} = 1.10192$
$d_{H_{39}-C_1} = 1.10192$	$d_{H_{40}-C_2} = 1.10192$

Table 2.5: Atomic positions and bond lengths for the $C_{18}H_{22}$ graphane NR in Å units.

Chapter 3

Theory

The scientific community has been interested in the development of theoretical approximations and also numerical methods to solve the quantum-mechanical problem of an interacting system consisting of electrons and nuclei. En general, this is a many body problem that can be solved with Density Functional Theory [22](**Hohenberg1964**). The solution of real systems is so challenging and is possible with the use of numerical methods. In particular, the methodology to find solutions for crystals is well developed and elaborated. Thus, in the present chapter, we just describe the main aspects of Density Functional Theory, which is used for the calculations. For further details, see, for instance, Reference [23](**Martin**).

3.1 Hamiltonian

The hamiltonian of a quantum system composed of atoms is

$$\begin{aligned}\hat{H} &= -\frac{\hbar^2}{2m_e}\sum \nabla_i^2 + \sum_{i,I}\frac{Z_I e^2}{|\mathbf{r}_i - \mathbf{R}_I|} + \frac{1}{2}\sum_{i\neq j}\frac{e^2}{|\mathbf{r}_i - \mathbf{r}_j|} - \frac{\hbar^2}{2M_I}\sum_I \nabla_I^2 + \frac{1}{2}\sum_{I\neq J}\frac{Z_I Z_J e^2}{|\mathbf{R}_I - \mathbf{R}_J|}, \\ &= \hat{T}_e + \hat{V}_{e-I} + \hat{V}_{e-e} + \hat{T}_I + \hat{V}_{I-I}, \end{aligned} \tag{3.1}$$

where each term on the right-hand side of the first line of equation (3.1) is denoted by $\hat{T}_e$, $\hat{V}_{e-I}$, $\hat{V}_{e-e}$, $\hat{T}_I$ and $\hat{V}_{I-I}$, respectively. $\hat{T}_e$ is the kinetic energy of the electrons, $\hat{V}_{e-I}$ is the potential due to the electron-ion interaction or external potential, $\hat{V}_{e-e}$ is the potential due to the electron-electron interaction, $\hat{T}_I$ is the kinetic energy of the ions and $\hat{V}_{I-I}$ is the potential due to the ion-ion interaction. Z_I is the atomic number of the I-th ion, $\mathbf{r}_i$ is the position of the i-th electron, $\mathbf{R}_I$ is the position of the I-th ion, m_e is the electron mass and $\hbar$ is the Planck constant.

In order to have a less complex form of the hamiltonian, some approximations can be done. Firstly, due to the considerable difference between the nucleous mass and the electron mass, and the immediate response of the electrons under nuclei movement, the kinetic energy of the nucleous can be considered as very small. In this manner, the movement of nuclei can be treated adiabatically. This leads to a separation of the nuclear and electronic coordinates in the wave function of the many body problem. This is known as Born-Oppenheimer approximation. It allows to reduce the many body problem to the problem of the dynamics of independent electrons. On the other hand, the ion-ion potential is a constant and can be left out of the equation for the hamiltonian. Thus, the hamiltonian reduces to three contributions.

$$\hat{H} = \hat{T}_e + \hat{V}_{e-I} + \hat{V}_{e-e}. \tag{3.2}$$

From now on, we change notation and write equation (3.3) in the form

$$\hat{H} = \hat{T} + \hat{V} + \hat{V}_{ext}. \tag{3.3}$$

where $T = T_e$, $\hat{V} = \hat{V}_{e-e}$ and $\hat{V}_{ext} = \hat{V}_{e-I}$.

3.2 Hohenberg-Kohn theorems

The Density Functional Theory was proposed by Hohenberg and Kohn in 1964 in their study of an inhomogeneous electron gas [22](**Hohenberg1964**). The main ideas of the theory can be summarized by the following two theorems.

Theorem 1: There is a one-to-one correspondence between the ground-state density $\rho(\mathbf{r})$ of a many-electron system and the external potential V_{ext} [22](**Hohenberg1964**).

Therefore so, the ground-state expectation value of any observable $\hat{O}$ is a unique functional of the exact ground-state electron density:

$$\langle \Psi \mid \hat{O} \mid \Psi \rangle = O[\rho]. \tag{3.4}$$

In particular, the external potential V_{ext} is a unique functional of ρ, apart from a trivial additive constant. Since, V_{ext} fixes $\hat{H}$, the ground state is a unique functional of the electron density ρ [22](**Hohenberg1964**).

The electron density is given by

$$\rho(\mathbf{r}) = \sum_{i=1}^{N} \phi_i(\mathbf{r})^* \phi_i(\mathbf{r}) \tag{3.5}$$

where $\phi_i(\mathbf{r})$ are the electron wave functions in state i.

Theorem 2: *Variational principle:* If $F[\rho(\mathbf{r})]$ were a known functional of $\rho(\mathbf{r})$, the ground-state energy and density in a given external potential is obtained by minimization of the functional of the density $\rho(\mathbf{r})$ [22](**Hohenberg1964**).

Being $\hat{O}$ the hamiltionian $\hat{H}$, the ground-state of the total energy functional $\hat{H}[\rho(\mathbf{r})] \equiv E[\rho(\mathbf{r})]$ is:

$$\begin{aligned} E[\rho(\mathbf{r})] &= T[\rho(\mathbf{r})] + E_C[\rho(\mathbf{r})] + E_{ext}[\rho(\mathbf{r})] \\ &= F_{HK}[\rho(\mathbf{r})] + E_{ext}[\rho(\mathbf{r})] \end{aligned} \tag{3.6}$$

where

$$F_{HK}[\rho(\mathbf{r})] = T[\rho(\mathbf{r})] + E_C[\rho(\mathbf{r})] = \langle \Psi \mid \hat{T} + \hat{V} \mid \Psi \rangle \tag{3.7}$$

is the Honhenberg-Kohn density functional, which is universal for any many-electron system; $T[\rho(\mathbf{r})]$ is the cinetic energy functional, $E_C[\rho(\mathbf{r})]$ is the Coulomb energy functional, and

$$E_{ext}[\rho(\mathbf{r})] = \langle \Psi \mid \hat{V}_{ext} \mid \Psi \rangle = \int V_{ext}(\mathbf{r})\rho(\mathbf{r})\mathrm{d}\mathbf{r} \tag{3.8}$$

is the external energy functional. The correct $\rho(\mathbf{r})$ gives the ground-state energy $E[\rho(\mathbf{r})]$. The minimal value of $E[\rho(\mathbf{r})]$ is equal to the ground-state total energy associated to the external potential V_{ext} and gives the correct $\rho(\mathbf{r})$ if the the following condition is satisfied

$$N[\rho(\mathbf{r})] = \int \rho(\mathbf{r})\mathrm{d}\mathbf{r} = N, \tag{3.9}$$

where N is the number of particles of the system.

There must exist more than one expression for the functional of the equation 3.7 for any many-electron system due to it does not depend on any nuclear variable, that is, it contains information only of the electrons of the system. Hence, the determination of the universal functional is a challenging task in many-electron systems.

3.3 The Kohn-Sham equations

Kohn and Sham, in 1965, followed the theory of Hohenberg and Kohn to treat and inhmogeneous systems of interacting particles [24](**Kohn1965**). They obtained self consistent equations which include, in an approximate way, the exchange and correlations energy terms, which arise due to the electron-electron interaction. On the one hand, the exchange energy is the reduction in the energy of a system due to the antisymmetry of the wave function under the exchange of any two electrons. The fact that the wave function is antisymmetric produces a spatial separation between electrons with the same spin, reducing the Coulomb energy of the system [25](**Payne1992**). On the other hand, in the case where the electrons have opposite spins, they will be also a spatial separation between electrons, and thus the coulomb energy is reduced below its Hartree-Fock value. Such a reduction is called correlation energy [25](**Payne1992**). Considering both, the exchange and the correlation effects, the exchange-correlation energy is given by:

$$E_{xc}[\rho(\mathbf{r})] = E_C[\rho(\mathbf{r})] - E_H[\rho(\mathbf{r})], \tag{3.10}$$

where $E_H[\rho(\mathbf{r})]$ is the Hartree energy. Hence, the total energy functional can be written as:

$$E[\rho(\mathbf{r})] = T[\rho(\mathbf{r})] + E_H[\rho(\mathbf{r})] + E_{xc}[\rho(\mathbf{r})] + E_{ext}[\rho(\mathbf{r})]. \tag{3.11}$$

The energy functional depends on two external potentials. The first one is the external interaction potential due to the presence of nuclei and the second one is that generated by the exchange-correlation effects. These effects contain extra information of the electron-electron interaction.

The Kohn-Sham hamiltonian corresponding to the energy functional is:

$$\hat{H}_{KS} = \hat{T} + \hat{V}_H + \hat{V}_{xc} + \hat{V}_{ext} \tag{3.12}$$

where

$$V_H(\mathbf{r}) = \frac{e^2}{4\pi\epsilon_0} \int \frac{\rho(\mathbf{r}')}{|\mathbf{r} - \mathbf{r}'|} d\mathbf{r}', \tag{3.13}$$

is the Hartree potential and V_{xc} is the exchange-correlation potential, which is given by:

$$V_{xc}(\mathbf{r}) = \frac{\delta E_{xc}[\rho]}{\delta \rho}. \tag{3.14}$$

From the Kohn-Sham hamiltonian it is possible to obtain the exact ground-state density by the mean of the Kohn-Sham theorem.

Kohn-Sham Theorem: For given electron wave function $\phi_i(\mathbf{r})$ and exchange-correlation potential $V_{xc}(\mathbf{r})$, the exact electron density $\rho(\mathbf{r})$ of the N electron system can be obtained by solving the Kohn-Sham equations

$$\hat{H}_{KS}\phi_i = \epsilon_i \phi_i. \tag{3.15}$$

where ϵ_i are the Kohn-Sham eigenvalues. The Kohn-Sham equations converts the problem of the interacting many-electron system to a problem of a system of noninteracting electrons inside and efective potential. Here, there is a selfconsistent problem: the Hartree potential V_{xc} and the exchange-correlation potential V_H depend on the electron density $\rho(\mathbf{r})$, and the electron density depends on the electron wave function solutions that we want to obtain. In this case, the density must be found self-consistently. Indeed, it must be consistent with the Kohn-Sham hamiltonian. The self-consistent solutions of the Kohn-Sham equations are those that minimize the Kohn-Sham total energy functional. At the minimum value, it is equal to the ground-state energy of the system.

3.4 Numerical method to get total energy

The computational procedure for the calculation of the total energy of a system composed of electrons and nuclei is that shown in Figure 3.1. Firstly, It is assumed and initial

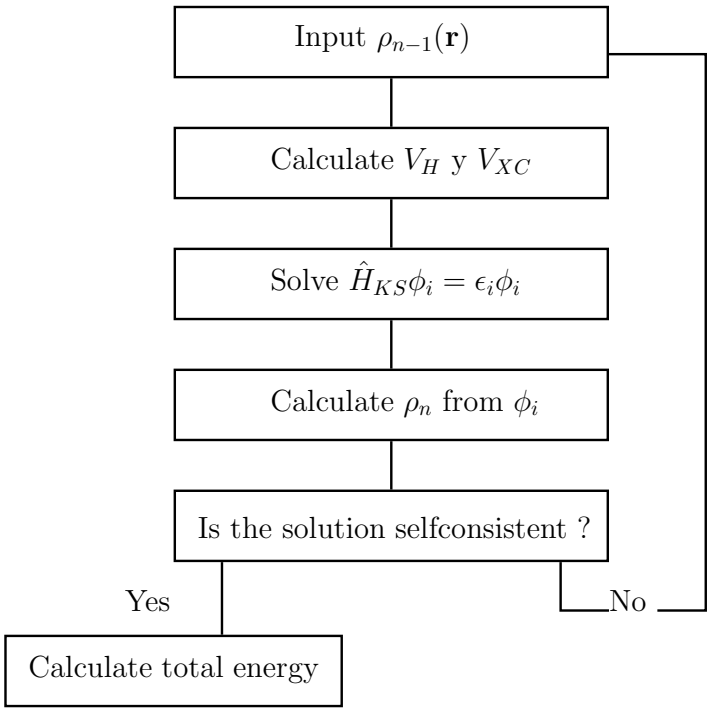

Figure 3.1: Procedure to calculate the total energy.

approximation to the electronic-charge density from which the Hartree and exchange-correlation potentials are constructed. Secondly, the Kohn-Sham hamiltonian of Equation (3.15) must be built. In order to solve it, the wave functions ϕ_i can be expressed in a given basis set ϕ_p^b in the form

$$\phi_m = \sum_{p=1} c_p^m \phi_p^b. \tag{3.16}$$

Hence, once equation (3.16) is substituted in the Kohn Sham equations (3.15), it is possible to obtain the matrix eigenvalue equation [26](**Cottenier2002**).

$$\begin{bmatrix} .. & .. & .. & .. \\ .. & \langle \phi_i^b \mid \hat{H}_{sp} \mid \phi_j^b \rangle - \epsilon_m \langle \phi_i^b \mid \phi_j^b \rangle & .. & .. \\ .. & .. & .. & .. \end{bmatrix} \begin{bmatrix} c_1^m \\ . \\ c_p^m \end{bmatrix} = \begin{bmatrix} 0 \\ . \\ 0 \end{bmatrix}. \tag{3.17}$$

The hamiltonian matrix for each point $\mathbf{k}$ is included in the calculation and once it is diagonalized the Kohn-Sham eigenstates, the eigenvalues are obtained. Then, the new charge density is calculated. The calculated eigenstates might generate different charge

density than that used in the construction of the electronic potentials. If that is the case, there is no a self-consistent solution. Thereupon, a new Kohn-Sham hamiltonian is built with the used of the calculated density. The procedure is repeated until the solution is self-consistent. Finally the total energy functional of equation (3.11) is calculated. Its value will correspond to the ground-state energy of the system (See discussion in the end of Section 3.3).

Chapter 4

Electronic properties

In this chapter, we present numerical calculations for the lattice constant and electronic band structure for graphite, graphene, graphane and graphane nanoribbons (NRs). We have used Density Functional Theory (DFT) within the Local Density Approximation. The calculations have been obtained by using the ABINIT code [27] that is based on pseudopotentials and plane waves. We focus in the convergence study of the lattice constant and electronic band structure in the parameters of the calculation such as cut-off energy, and number of **k** points n_k[1]. It is worth to address that a convergence study allows to obtain the value of a parameter of the calculus that make the quantity under study, here the lattice constant and energy bands, to tend to a definite limit value. For the calculation, we have used the corresponding atomic structures described and calculated in Chapter 2.

4.1 Parameters of the calculation

In the calculation of the lattice constant and bandstructure of for graphite, graphene, graphane and graphane nanoribbons (NRs), we have considered the following considerations. The used pseudotentials were the relativistic separable dual-space Gaussian pseudopotentials of Hartwigsen-Goedecker-Hutter [28]. We considered 4 valence bands for the carbon atom pseudpotential. Spin-orbit (SO) interaccion was not taken into ac-

[1]The cut-off energy defines the number of planes waves used for the wave function, and n_k defines the number of **k** points used to calculate the self-consistent ground state.

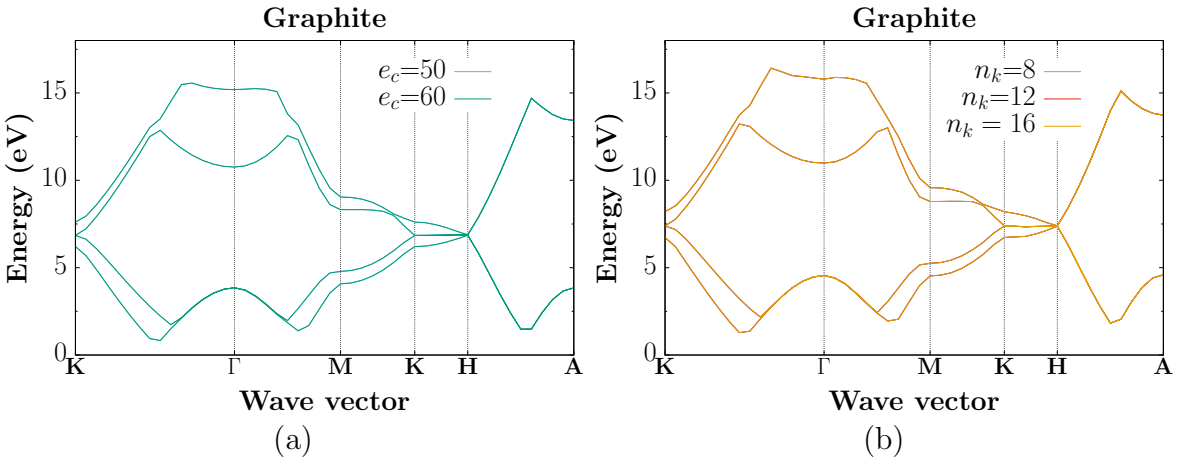

Figure 4.1: The convergence study of the two higher valence and two lower conduction bands in the cut-off energy e_c (a), and in the number of **k** points n_k (b).

count. The monolayer structure of graphane and the graphane NRs were modeled by using a supercell approach. A vaccum lenght of at least 8.22 Å was considered.

4.2 Graphite

The bulk structure of Graphite was described in Section 2.3. Here, we have obtained the electronic band structure for graphite. Firstly, we have done a convergence study of the two higher valence and two lower conduction bands in the cut-off energy e_c. Through this process, we calculated the energy bands for various values of e_c. We came to the conclusion that the corresponding valence and conduction bands for graphite with cut-off energies of 50 and 60 eV, respectively, overlap as it is shown in Figure 4.1(a). Therefore, we used $e_c = 50$ eV for the calculation of the band structure and for the convergence study in the number of **k** points. For that, we took $n_k = 8, 12$, and 16. It can be seen in Figure 4.1(b) that the corresponding energy bands are overlapped. Consequently, in the following, the band structure calculations of this material are done with 8 **k** points.

We show in Figure 4.2, the converged band structure without spin orbit (SO) interaction of graphite along the path that join the high symmetry **k** points K, Γ, M, K, H, and A. This material is classified as a metal or semimetal, due to the fact that at **K** and along the path K-H the maximum valence band values equal to the minimum conduction band values. In other words, graphite does not have an energy band gap. In Figure 4.2,

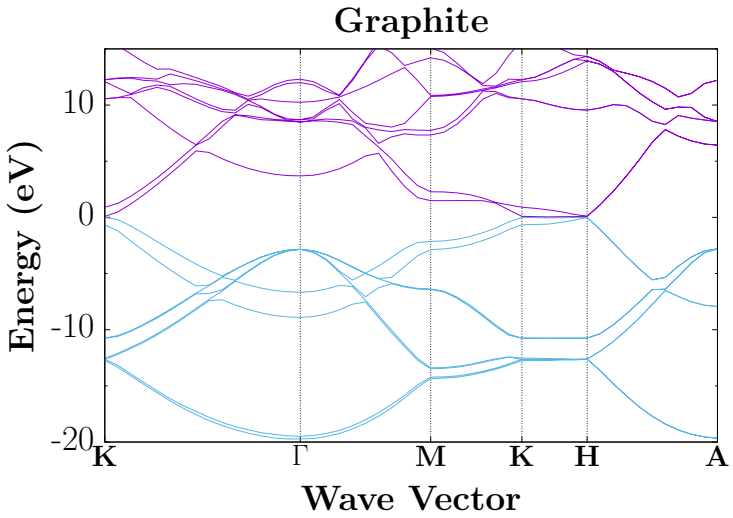

Figure 4.2: Band structure of graphite. The blue lines are valence bands and the purple lines are the conduction bands.

it can be seen that there are eight valence bands that are shown in blue. The minimum of the first valence band is found at the Γ point and the maximum of the heighest valence band is at the K point.

4.3 Graphene

The monolayer structure of graphene was described in Section 2.4. In order to see how its lattice constant was obtained, we executed a convergence study in the cut-off energy and the number of **k** points. Firstly, we took cut-off energy values of 140 and 160 eV. In Fig 4.3(a), we can observe that the lowest total energy value is 2.443 Å . Therefore, we used 140 eV for the cut-off energy parameter to determine the convergence study in the numer of **k** points. On the other hand, we took different number of **k** points for the ground state calculation, $n_k = 8, 12, 16, 20,$ and 24 We note that, although all corresponding curves changes in magnitude, the lowest value for all the curves keeps the same vaue of 2.443 Å . Thus it is just enough to consider in the calculation $n_k = 8$.

We have also performed a convergence study of the energy bands for graphene just as in the case of graphite. Thus, in Figure 4.4, we show the converged band structure without spin orbit (SO) interaction of graphene along high symmetry wave vector points. We can see that the graphene is a semimetal material just as graphite is. At the K and H

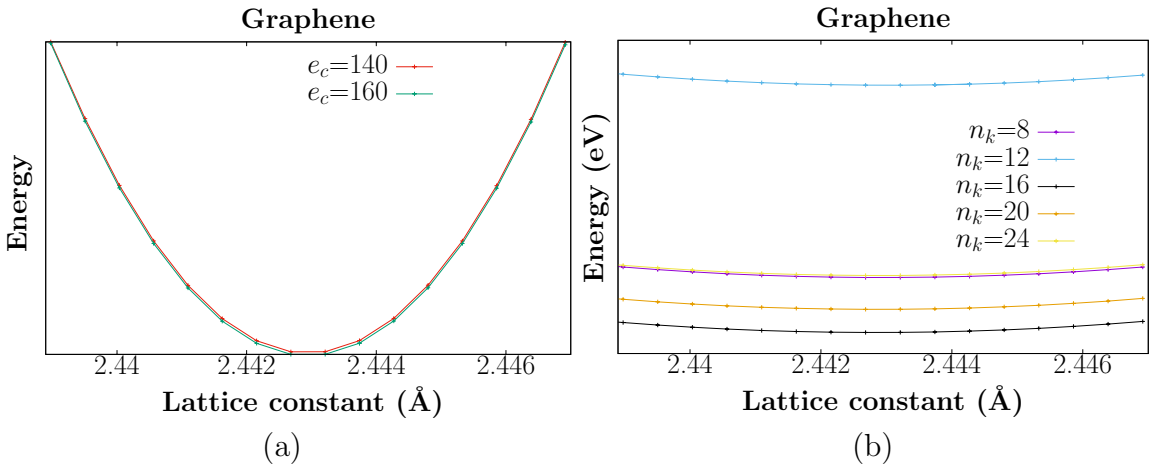

Figure 4.3: Convergence study of the lattice constant of graphene of the two higher valence and two lower conduction bands in the cut-off energy e_c (a), and in the number of **k** points n_k.

high symmetry points, the maximum valence band joins the minimum conduction band. You can distinguish that graphene has four valence bands that are shown by the blue lines. The minimum of the first valence band is found at Γ and the maximum of the heighest valence band is at the K point.

4.4 Graphane

We have already described the atomic structure of graphane in Section 2.5. Performing total energy minimization, we have obtained its atomic structure. We calculated an interatomic bonding of d_{CC} =1.513 Å , d_{CH} =1.116 Å and the lattice constant is equal to 2.505 Å. Our results are comparable with those calculations reported by Sahin [19](**Ataca2010**), who obtained the following values: d_{CC} =1.52 Å , d_{CH} =1.12 Å and 2.516 Å for the lattice constant.

Here, in Figure 4.5(a), the graphane band structure is shown along the high symmetry points indicated by K, Γ, M, K, H and A. This material is classified as a semiconductor due to it has an energy band gap, which is direct and has the value of 3.391 eV. We can observe from the Figure that there are five valence bands. The minimum of the first valence band is found at Γ, and the maximum of the heighest valence band is also at the Γ point. The minimum of the first conduction band is found at the Γ point. The two top valence bands at around Γ are very sensitive to small changes of the positions of

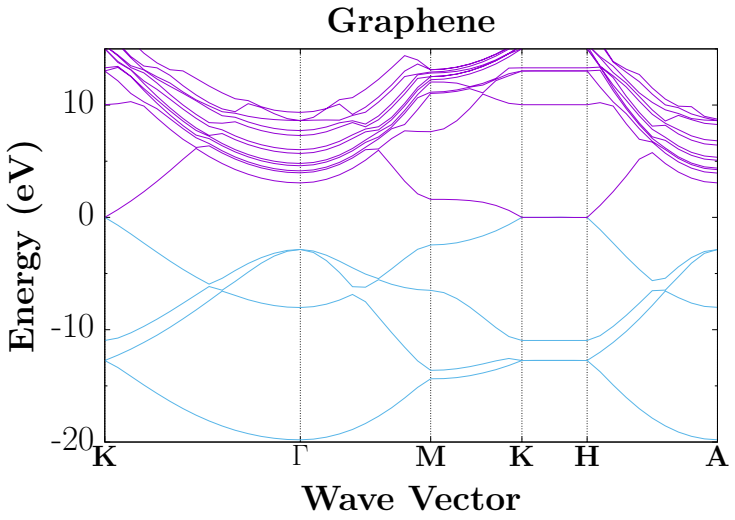

Figure 4.4: The band structure of the graphene where the blue lines are valence bands and the purple lines are conduction bands.

the atoms. We show this in Figure 4.5(b). Here, the band structure correspond to the relaxed bandstructure where the atom postions were shifted slightly along the x direction by small amount of 0.00599 Å . Comparing both bandstructures of Figure 4.5, we can observe that, at Γ, the two top valence bands do not overlap for the case were the atoms positions were shifted from those of the relaxed structure. In contrast, the two top valence bands do overlap in the banstructure corresponding to the relaxed structure. Besides, the the band gap energy has the value of 3.07 eV for the graphane structure were the atoms were shifted. Such differences are reflected in the linear optical response spectrum (see Section 5.2). This suggest that a well converged atomic structure is requiered in order to obtain the correct bandstructure. The band structure of graphane seen in Figure 4.5(a) is comparable to others already reported [15, 20, 13](**Sofo2007,Yang2012,Sahhin2015**).

4.5 Graphane nanoribbons

We have also relaxation of the atoms and calculation of the the electronic band structure of armchair graphane NRs: C_6H_{10}, $C_{10}H_{14}$, $C_{14}H_{18}$, $C_{18}H_{22}$. Their corresponding unit cell structures were described in Section 2.6. The relaxation of the structure results in the values of the lattice constant and width of the studied NRs tabulated in Table 4.1 The respective band structures for the studied graphane NRs along high symmetry points indicated by Γ and M are shown in Figure 4.6. There are 17, 27, 37, and 47 valence bands

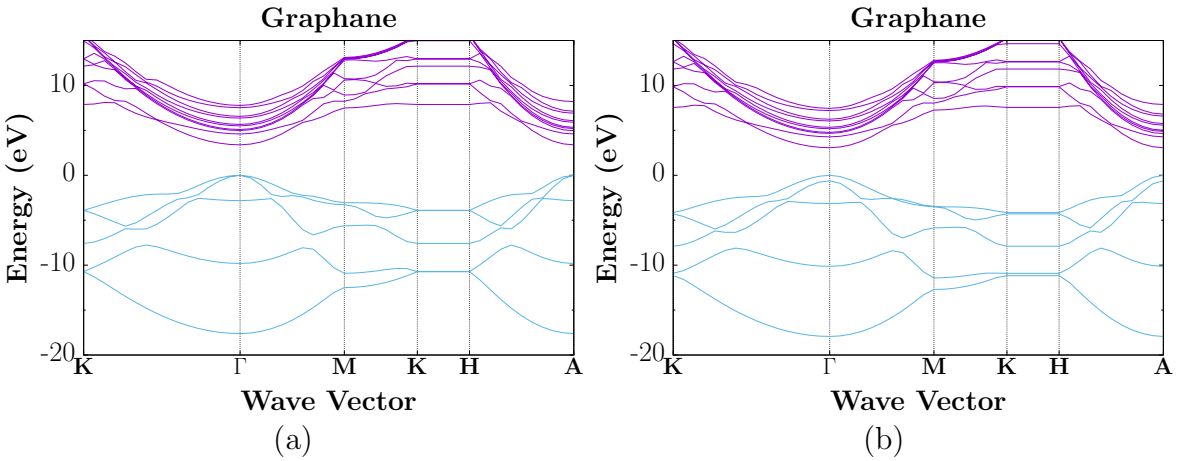

Figure 4.5: Band structure of graphane, where the blue lines are valence bands and the purple lines are conduction bands. In (a) the band structure correspond to the relaxed graphane structure, and in b) it is obtained by shifting the atomic positions of the relaxed graphane structure along the x direction by a small amount of 0.00599 Å.

in the bandstructures of the C_6H_{10}, $C_{10}H_{14}$, $C_{14}H_{18}$, $C_{18}H_{22}$ graphane NRs, respectively. In all the band structures, the minimum of the first valence band is found at Γ, the maximum of the heighest valence band is also at the Γ point, and the minimum of the first conduction band is found at the Γ point. The studied graphane NRs are classified as semiconductors since they have a direct energy band gap whose values are 5.391, 4.605, 4.200 and 3.961 eV for the C_6H_{10}, $C_{10}H_{14}$, $C_{14}H_{18}$, $C_{18}H_{22}$ graphane NRs, respectively (see Table 4.1). We can also see from Figure 4.6, that all bandstructures of the studied graphane NRs mainly contain planar bands indicating that there is small dispersion. Besides, we note that there are a high density of band states in a small interval range of energy both below and above the energy band gap.

In Figure 4.7, we plot the energy band gap as a function of the width of the studied

Graphane NRs	Lattice constant (Å)	Width (Å)	Band gap energy (eV)
C_6H_{10}	4.4115	2.465	5.391
$C_{10}H_{14}$	4.3752	4.975	4.605
$C_{14}H_{18}$	4.3632	7.482	4.200
$C_{18}H_{22}$	4.3573	9.988	3.961

Table 4.1: Lattice constant, width and band gap energy of the studied NRs.

armchair graphane NRs. We also compare our LDA calculations shown in red with those GGA results done by Yang et al. [20](**Yang2012**) shown in blue. The data are join with lines in order to see the behavior of the energy band gap. We can see from the figure that the band gap energy decreases as the width of the NR increases. It takes values from 5.391 eV for C_6H_{10} graphane NR and decreases to the value of 3.961 eV for the $C_{18}H_{22}$ graphane NR.

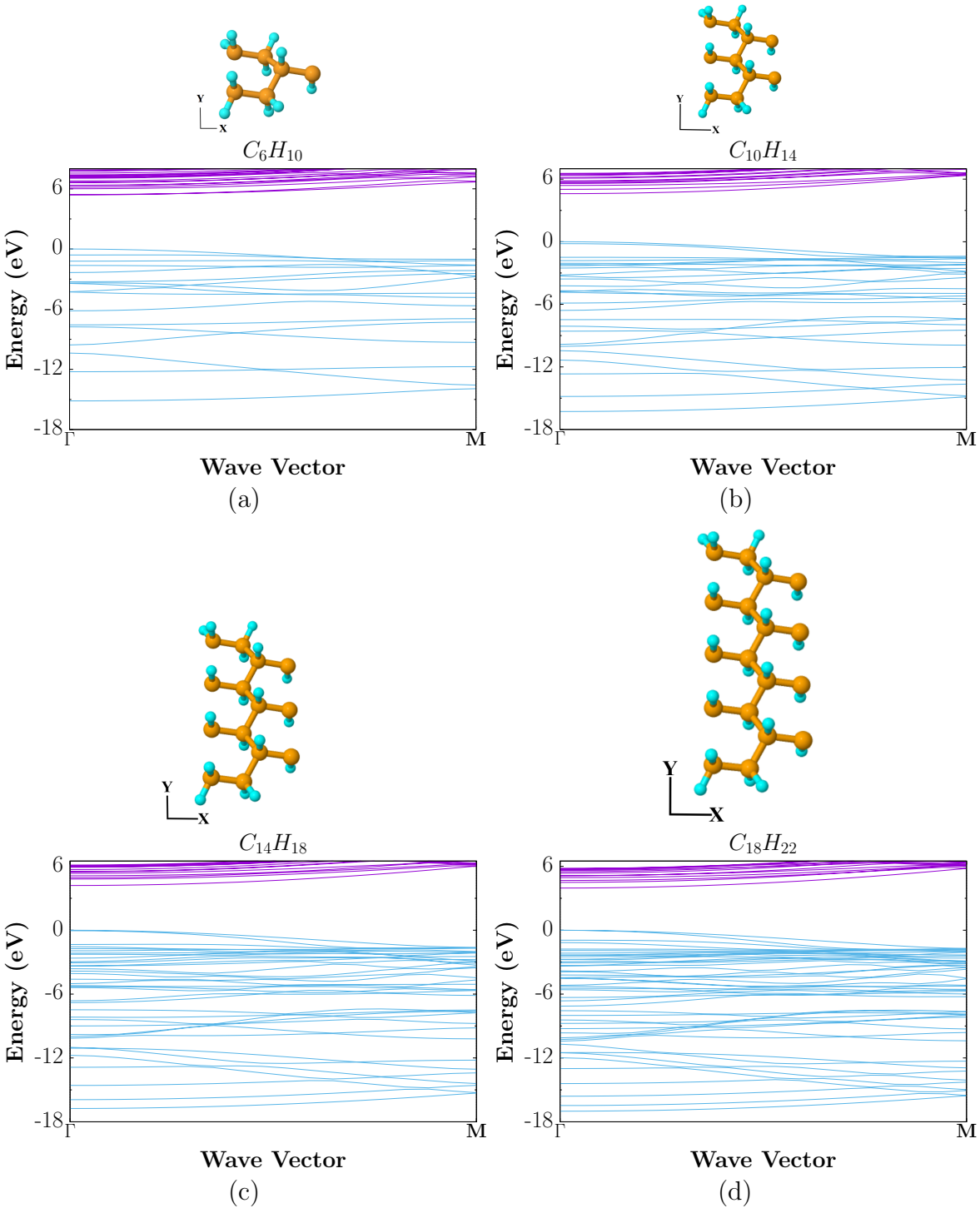

Figure 4.6: Band structures of the studied armchair graphane NRs: C_6H_{10}, $C_{10}H_{14}$, $C_{14}H_{18}$, and $C_{18}H_{22}$.

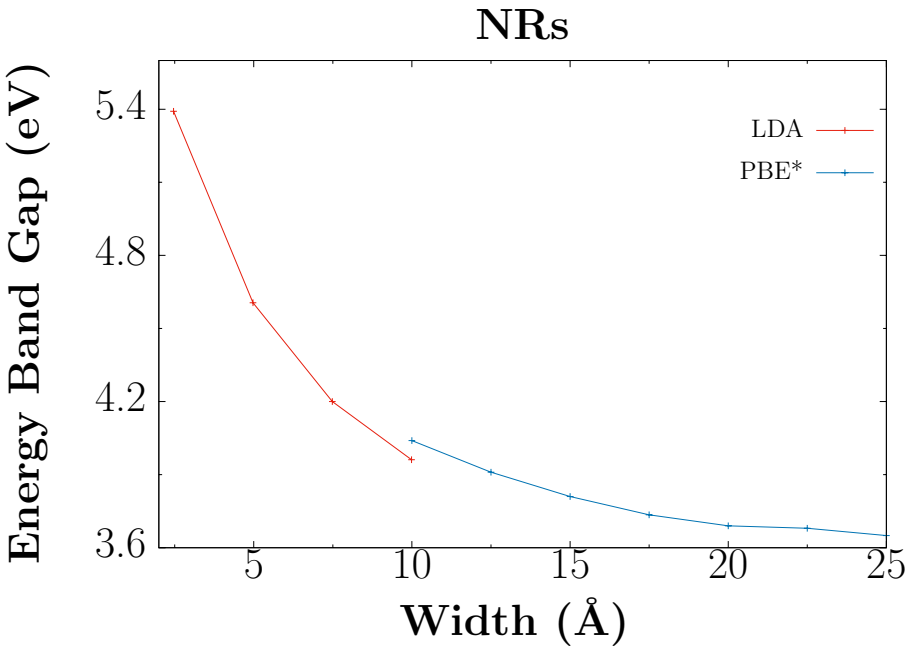

Figure 4.7: Plot of the energy band gap as a function of the width of the studied armchair graphane NRs. We compare our LDA calculated results shown in red with those GGA results calculated by Yang et al. which are shown in blue.

Chapter 5

Optical response

In this chapter, we present numerical calculations for the linear optical response of graphane and the studied graphane nanoribbons (NRs). Graphane nanoribbons exhibit important number of properties and hence constitute basic structures to fabricate various devices. The different NRs are wide band-gap semiconductor when their edges are passivated with hydrogen [19](**Ataca2010**). The studied graphane NRs are described in Section 2.6.

5.1 Method

Firstly, both graphane and graphane NRs structures were modeled by using a supercell approach. A vaccum lenght of at least 8.23 Å was considered. We have used Density Functional Theory (DFT) within the Local Density Approximation. The calculations have been obtained by using the ABINIT code [27](**abinit**) for obtaining wavefunctions and eigenenergies, with the use of pseupotentials and planewaves. The ion-core potential was replaced by the relativistic separable dual-space Gaussian pseudopotentials of Hartwigsen-Goedecker-Hutter [28](**Hartwigsen1998**). We considered 4 valence bands for the carbon atom pseudopotential. Spin-orbit (SO) interaccion was not taken into account. We have taken a cut-off energy of 60 Ha for the plane wave expansion of the wave functions and used 8 **k** points for the ground state calculation. For the optics calculation, the linear tetrahedra method was used where 300 **k** point were used in the irreducible Brillouin zone. The number of bands considered in the calculation was 200.

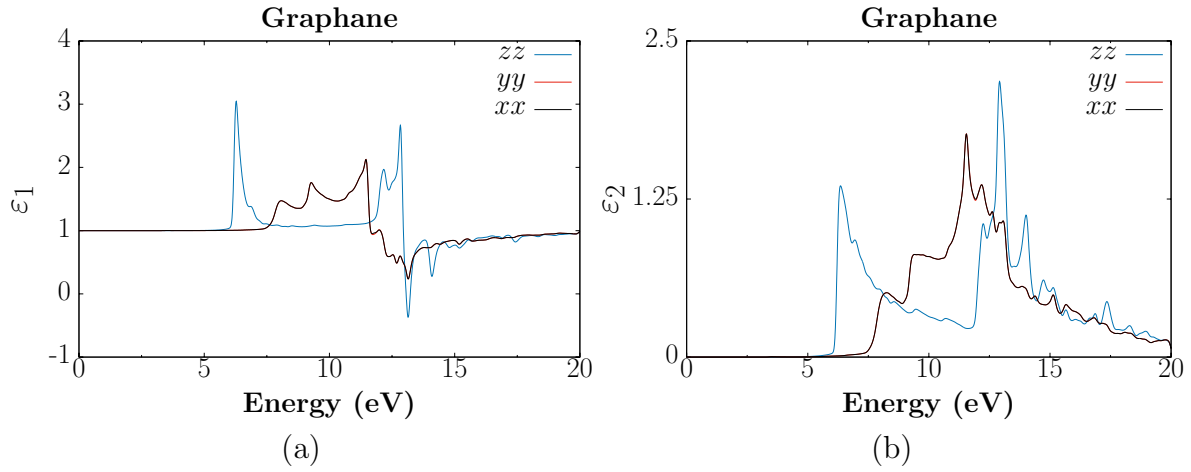

Figure 5.1: Real (a) and imaginary (b) parts of of the dielectric function for graphane.

Our calculation has the characteristic of being a full-band structure calculation, that is it takes into account the contributions to the spectrum of **k** points in the whole Brillouin zone.

5.2 Graphane

The spectra of the real and imaginary parts of the dielectric function for graphane are shown in Figure 5.1. We observe that the spectra shows isotropy on the plane of the monolayer, but it shows anisotropy in the responses pararell (xx, or yy) and perpendicular (zz) to the plane of atomic structure. We also observe from Figure 5.1(b) that the absorption spectra starts having appreciable values well above the band gap value of 3.391 eV. When the spectrum has zero values at some frequency there is no absorption because the photon energy is within the energy band gap or the material is transparent to that frequencies. In particular, the imaginary part of the dielectric function component ϵ_{zz} exhibits two main absorption peaks, which are at 6.20 eV and 13.19 eV, respectively. While for ϵ_{xx} and ϵ_{yy} it exhibits a peak which is at 11.41 eV.

Small deviations of the atom positions might result in the loss of the structural symmetry of the crystal. This is shown in Figure 5.2, where the imaginary parts of the dielectric function for parallel (xx and yy) and perpendicular (zz) light polarizations are plotted for the relaxed graphane structure having their atom positions shifted along the x direction by 0.00599 Å. Here, we see that the corresponding spectra of ϵ_{xx} and ϵ_{xy} do not

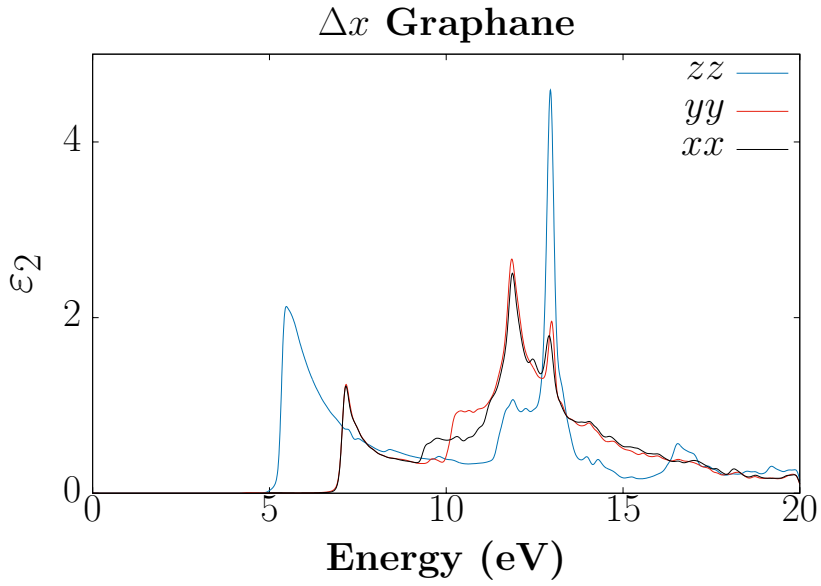

Figure 5.2: The imaginary portion, ε_2, of the dielectric function for graphane.

overlap, which mean that the optical response turns to be anisotropic on the plane of the graphane structure. This, Indeed, is not correct for an hexagonal layered system, which must be isotropic as it is shown in Figure 5.1(b). The corresponding band structures of relaxed graphane structure and of the relaxed graphane with shifted atom positions are shown in Figure 4.5. The most visible difference between both bandstructures is seen in the two top valence bands at around Γ. Such a difference is not reflected in the optical spectrum since the optical transitions that must contribute to the spectrum are just above the band gap energy. Very slight differences might be present in the energy bands, which, in turn, are reflected in the optical spectrum.

5.3 Armchair graphane nanoribbons

In this section, we show results for the optical response of the studied armchair graphane NRs. Firstly, we analyze the reliability of the calculations for high frequencies in terms of the transitions that contribute to the spectrum. In other words the number of bands in the calculation plays a main role in the spectrum for high frequencies. We see in Figure 5.3, spectra for the imaginary part of the dielectric function as a function of the number of bands that are taken in the DFT calculation. We can observe the great difference between spectra with number of bands of $n_b = 50$ and $n_b = 200$ for photon energies

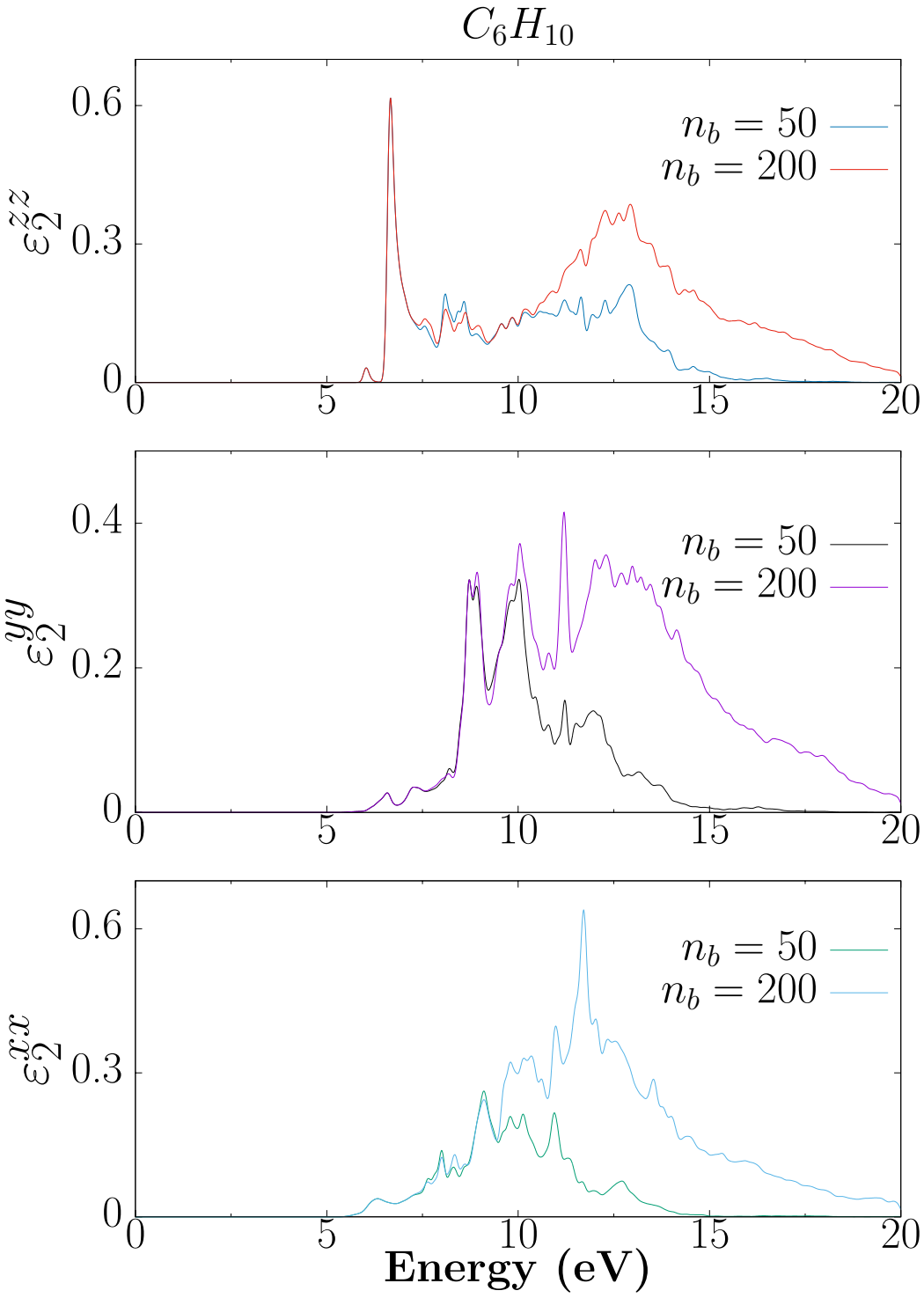

Figure 5.3: Spectra of the imaginary part ε_2 of the dielectric function for the C_6H_{10} graphane NRs for a number of bands n_b equal to 50 and 200.

above 10 eV. Indeed, as long as we take more states in the calculation more high-energy transitions contribute to the spectrum.

We show in Figure 5.4 converged spectra for the imaginary part ε_2 of the dielectric function for C_6H_{10}, $C_{10}H_{14}$, $C_{14}H_{18}$ and $C_{18}H_{22}$ NRs. We see in all spectra, that they start having appreciable values different from zero above 5 eV. In the case of the C_6H_{10} graphane NR (Figure 5.4(a)). The spectrum for ϵ_2^{zz} component exhibits two main peaks at 6.33 eV and 12.93 eV, respectively. While for ϵ_2^{yy} has a peak at 11.29 eV and ϵ_2^{xx} presents a peak at 11.99 eV. In Figure 5.4(b), we see corresponding results for the $C_{10}H_{14}$ graphane NR. The spectrum for the ϵ_2^{zz} component exhibits two main peaks, at 6.31 eV and 12.67 eV, respectively. While ϵ_2^{yy} has a peak at 11.87 eV and ϵ_2^{xx} presents two main peaks at 11.99 eV and 12.21 eV. We can see in Figure 5.4(c) the respective optical response of the $C_{14}H_{18}$ graphane NR. The spectrum for ϵ_2^{zz} component exhibits three main peaks at 6.30, 6.78, and 13.18 eV, respectively. While ϵ_2^{yy} show a peak at 13.16 eV and ϵ_2^{xx} has a peak at 12.38 eV. The optical response for the $C_{18}H_{22}$ graphane NR is shown in 5.4(d). We se that the spectrum for ϵ_2^{zz} exhibits two main peaks at 6.25 eV and 13.06 eV, respectively. ϵ_2^{yy} has a peak at 12.14 eV and ϵ_2^{xx} presents a peak at 12.38 eV.

We also see from Figure 5.4 that the optical response of the armchair graphane NRs is anisotropic in the three spatial directions. This is the expected behavior due to symmetry reasons. The NRs are structurally different in the three spatial directions. The NR structure is infinite and periodical in the x direccion, and it is finite with different widths in the y and z directions.

In Figure 5.5, we show spectra for the three components different from zero of the imaginary part of the dielectric function ϵ_2^{xx}, ϵ_2^{yy} and ϵ_2^{zz} as a function of the NR structure. We see the general tendency that as the width of the NR increases, the respective spectrum of the NR approaches that of graphane. Indeed, this is the expected behavior of the optical response.

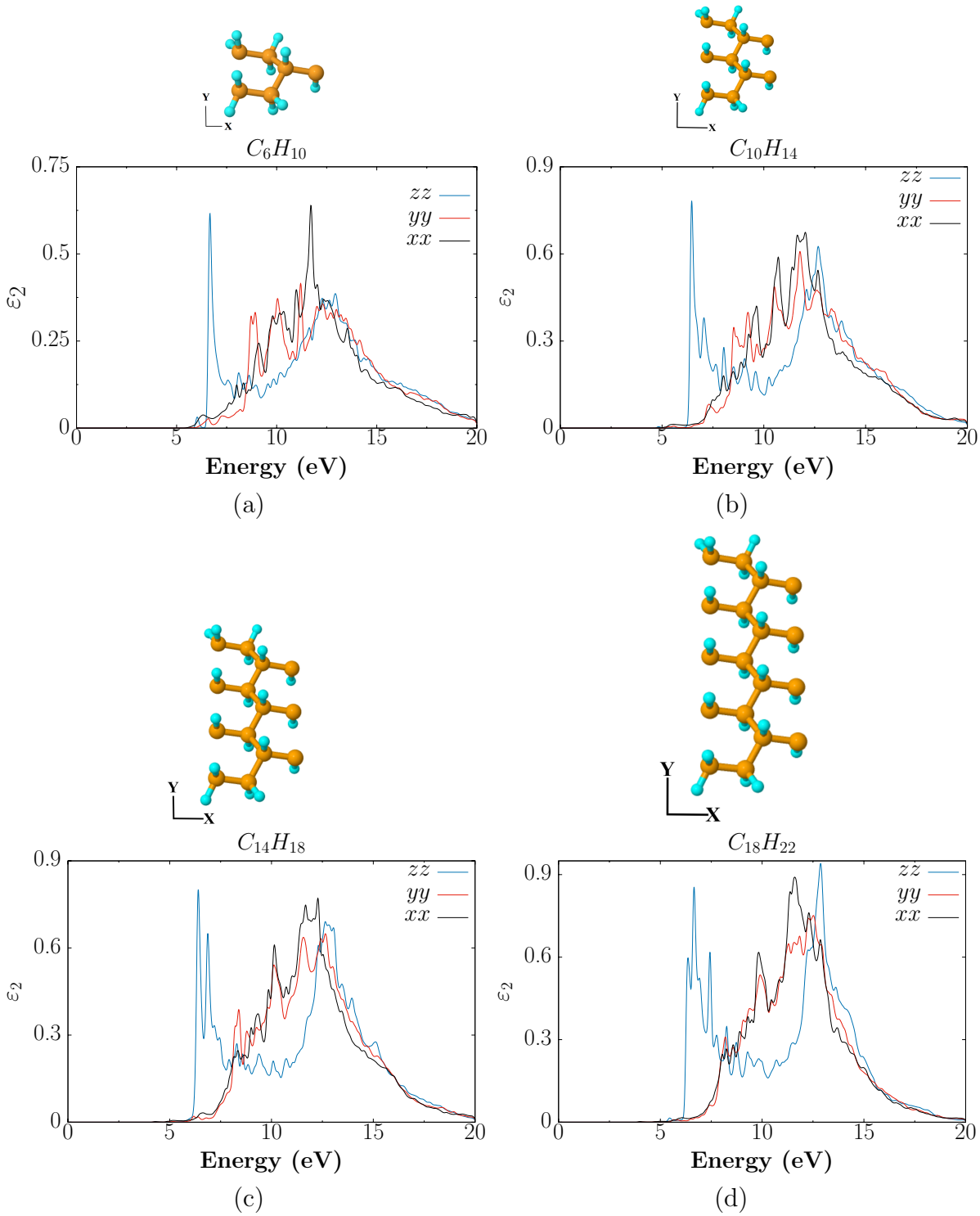

Figure 5.4: Spectra of the imaginary part ε_2 of the dielectric function for the studied graphane NRs.

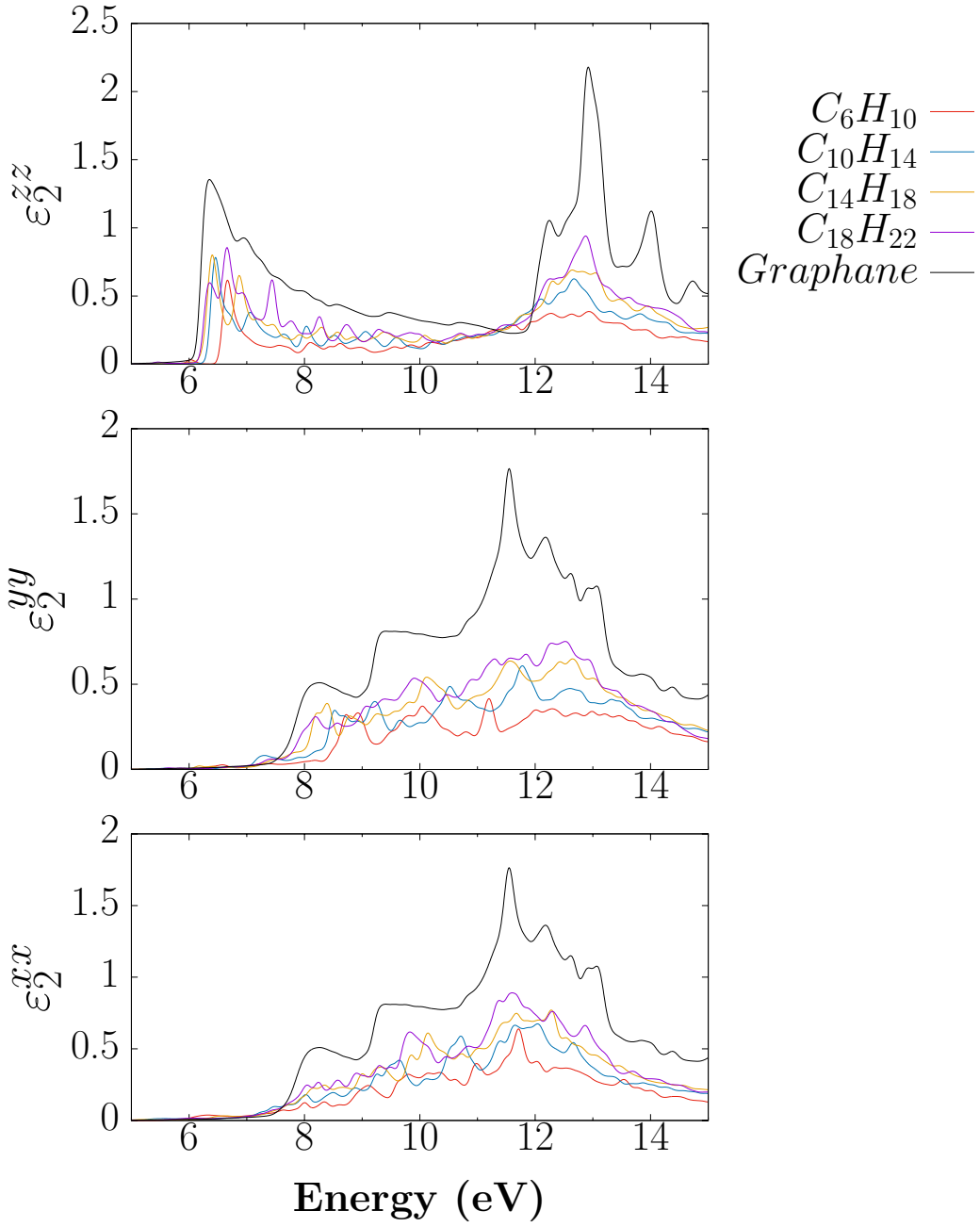

Figure 5.5: Spectra of ϵ_2^{xx}, ϵ_2^{yy} and ϵ_2^{zz} as a function of the NR structure.

Chapter 6

Conclusions

We have perfomed a theoretical study of the electronic properties and optical response of graphane and the following armchair graphane nanoribbons (NRs): C_6H_{10}, $C_{10}H_{14}$, $C_{14}H_{18}$ and $C_{18}H_{22}$. Firstly, in order to form the atomic arrangement of the studied structures, the primitive and reciprocal vectors of an hexagonal lattice were obtained. Then we perfomed a full relaxation of the structures and obtained the corresponding lattice constant for graphene, graphane and graphane NRs. The lattice constant for C_6H_{10}, $C_{10}H_{14}$, $C_{14}H_{18}$ and $C_{18}H_{22}$ NRs are 4.4115, 4.3752, 17.5279 and 20.0344 Å , respectively. Then, the corresponding electronic band structures, as well as the optical responses were calculated for graphane and the studied graphane NRs. An important step in our study was the convergence study, which was also performed for the energy bands.

We have found that, graphane and the graphane NRs are semiconductor materials, in contrast to graphite and graphene which are conductor materials. The band gap energy of armchair graphane NRs decreases as the width of the NR increases. The band gap energies are 5.391 eV for the C_6H_{10} NR, 4.605 eV for the $C_{10}H_{14}$ NR, 4.200 eV for the $C_{14}H_{18}$ NR and 3.961 eV for $C_{18}H_{22}$ NR.

We found that the lineshape of the spectrum of the imaginary part of the dielectric function of graphane NRs is similar to that of graphane. However, it shows an overall decreasing of its magnitude in the whole range of frequencies as the NR width reduces. The imaginary part of the dielectric function for ϵ_{zz} of the $C_{14}H_{18}$ NR have their largest peaks at 6.30 eV, 6.78 eV and 13.18 eV. While ϵ_{yy} exhibits a peak which is at 13.16 eV.

With regard to the ϵ_{xx} component both structures $C_{18}H_{22}$ and $C_{14}H_{18}$ present a largest peak at around of 12.38 eV. Finally, we confirm our hypothesis stated that the optical response of graphane nanostructures in the form of NRs is anisotropic.

Appendix A

Abbreviations and variables

BZ	Brillouin zone
d_{CC}	Carbon-carbon bond length
d_{CH}	Carbon-hydrogen bond length
DFT	Density Functional Theory
e	Electrons
e_c	Cut-off energy
$F_{HK}[\rho]$	Honhenberg-Kohn density functional
$\hat{H}$	Hamiltionian
$\hat{H}_{KS}$	Kohn-Sham hamiltonian
I	Nuclei or ions
n_b	Number of bands
n_k	Number of k-points
LDA	Local Density Approximation
NRs	Nanoribbons
$\hat{O}$	Observable
ϕ_i	Eigenfunctions from the perturbed system
$\rho(\mathbf{r})$	Ground-state density
$\mathbf{r}_i$	Position of the i-th electron
$\hat{T}$	Kinetic energy of the electron gas
T	Exact kinetic energy functional
T_0	Kinetic energy functional of a non-interacting electron gas
$\hat{T}_e$	Kinetic energy of the electrons
$\hat{T}_I$	Kinetic energy of the ions
V	Electron-electron potential energy functional
$\hat{V}_{e-e}$	Potential due to the electron-electron interaction

$\hat{V}_{e-I}$	Potential due to the electron-ion interaction
$\hat{V}_{I-I}$	Potential due to the ion-ion interaction
V_{ext}	External potential
$V_{xc}(\mathbf{r})$	Exchange-correlation potential
Z_I	Atomic number of the i-th electron
1D	One dimensional
2D	Two dimensional
3D	Three dimensional

Bibliography

[1] K. S. Novoselov, A. K. Geim, S. V. Morozov, D. Jiang, Y. Zhang, S. V. Dubonos, I. V. Grigorieva, and A. A. Firsov, *Electric field effect in atomically thin carbon films*, Science **306**(5696), 666 (2004).

[2] K. S. Novoselov, D. Jiang, F. Shedin, T. J. Booth, V. V. Khotkevich, S. V. Morozov, and A. K. Geim, *Two-dimensional atomic crystals*, PNAS **102**(30), 10451 (2005).

[3] F. Xia, H. Wang, and Y. Jia, *Rediscovering black phosphorus as an anisotropic layered material for optoelectronics and electronics*, NATURE COMMUNICATIONS **5**(4458), 1 (2014).

[4] F. Xia, H. Wang, D. Xiao, M. Dubey, and A. Ramasubramaniam, *Two-dimensional material nanophotonics*, nature photonics **8**, 899 (2014).

[5] A. F. Morpurgo, *The abc of 2d materials*, Nature Physics **11**, 625 (2015).

[6] V. Singh, D. Joung, L. Zhai, S. Das, S. Khondaker, and S. Seal, *Graphene based materials: Past, present and future*, Progress in Materials Science **8**(56), 1178 (2011).

[7] A. H. C. Neto, F. Guinea, N. M. R. Peres, K. S. Novoselov, and A. Geim, *The electronic properties of graphene*, Rev. Mod. Phys. **81**(1), 109 (2009).

[8] M. G. M. Medrano, H. Rosu, and L. González, *Grafeno: el alótropo más prometedor del carbono*, Acta Universitaria **22**(3), 20 (2012).

[9] V. Singh, D. Joung, L. Zhai, S. Das, S. Khondaker, and S. Seal, *Graphene based materials: Past, present and future*, Progress in Materials Science **8**(56), 1178 (2011).

[10] A. H. C. Neto and K. Novoselov, *Two-dimensional crystals: Beyond graphene*, Mater.Express **1**(1), 2158 (2011).

[11] K. Rodriguez, A.Sáenz, L. Barajas, L. Farías, and R. M. Jiménez, *Graphene: Properties and applications*, Acta Quimica Mexicana (13) (2015).

[12] E. V. Castro, K. S. Novoselov, S. V. Morozov, N. M. R. Peres, J. M. B. L. dos Santos, J. Nilsson, F. Guinea, A. K. Geim, and A. H. C. Neto, *Biased bilayer graphene: Semiconductor with a gap tunable by the electric field effect*, Phys.Rev.Lett. **99**(21), 216802 (2007).

[13] H. Sahin, O. Leenaerts, S. K. Singh, and F. M. Peeters, *Graphane*, Comput Mol Sci **5**, 255 (2015).

[14] M. Craciun, S. Russo, M. Yamamoto, J. Oostinga, A. Morpurgo, and S. Tarucha, *Trilayer graphene is a semimetal with a gate-tunable band overlap*, Nature Nanotechnology **4**(6), 383 (2009).

[15] J. O. Sofo, A. S. Chaudhari, and G. D. Barber, *Graphane: A two-dimensional hydrocarbon*, Phys. Rev. B **75**(15), 153401 (2007).

[16] D. C. Elias, R. Nair, T. M. G. Mohiuddin, S. V. Morozov, P. Blake, M. P. Halsall, A. C. Ferrari, D. W. Boukhvalov, M. I. Katsnelson, A. K. Geim, *et al.*, *Control of graphene's properties by reversible hydrogenation: Evidence for graphane*, Science **323**(5914), 610 (2009).

[17] H. C. Huang, S. Y. Lin, C. L. Wu, and M. F. Lin, *Configuration- and concentration-dependent electronic properties of hydrogenated graphene*, Carbon **103**, 84 (2016).

[18] H. Sahin, O. Leenaerts, S. K. Singh, and F. M. Peeters, *GraphAne: from synthesis to applications*, ResearchGate (2015).

[19] H. Sahin, C. Ataca, and S. Ciraci, *Electronic and magnetic properties of graphane nanoribbons*, Phys. Rev. B **81**(20), 205417 (2010).

[20] Y. Yang, Y. Yang, and X. Yan, *Universal optical properties of graphane nanoribbons: A first-principles study*, Physica E **44**, 1406 (2010).

[21] J. Hu, J. Zhang, S. Wu, and Z. Zhu, *Hybrid functional studies on the optical and electronic properties of graphane and silicane*, Solid State Communications **209-210**, 59 (2015).

[22] P. Hohenberg and W. Kohn, *Inhomogeneous electron gas*, Phys. Rev. **136**(3B), 864 (1964).

[23] R. M. Martin, *Electronic structure, basic theory and practical methods*, Cambridge University Press, (2004).

[24] W. Kohn and L. J. Sham, *Self-consistent equations including exchange and correlation effects*, Phys. Rev. **140**(4A), 1133 (1965).

[25] M. C. Payne, M. P. Teter, D. C. Allan, T. A. Arias, and J. D. Joannopoulos, *Iterative minimization techniques for ab initio total-energy calculations: molecular dynamics and conjugate gradients*, Rewiews of Modern Physics **64**(4), 1046 (1992).

[26] S.Cottenier, *Density functional theory and the family of (L)APW-methods: a step-by-step in- troduction*, (Instituut voor Kern- en Stralingsfysica, K.U.Leuven, Belgium), 2002, ISBN 90-807215-1-4 (to be found at http://www.wien2k.at/reg user/textbooks).

[27] Abinit, home page: http://www.abinit.org.

[28] C.Hartwigsen, S. Goedecker, and J. Hutter, *Relativistic separable dual-space gaussian pseudopotentials from H to Rn*, Phys. Rev. B **58**(7), 3641 (1998).